PCCP

PAPER

View Article Online
View Journal | View Issue

Cite this: *Phys. Chem. Chem. Phys.*, 2014, **16**, 9831

Structural and dynamical characteristics of trehalose and sucrose matrices at different hydration levels as probed by FTIR and high-field EPR

M. Malferrari,[a] A. Nalepa,[b] G. Venturoli,[ac] F. Francia,[a] W. Lubitz,[b] K. Möbius[bd] and A. Savitsky*[b]

Received 24th September 2013,
Accepted 26th November 2013

DOI: 10.1039/c3cp54043j

www.rsc.org/pccp

Some organisms can survive complete dehydration and high temperatures by adopting an *anhydrobiotic* state in which the intracellular medium contains large amounts of disaccharides, particularly trehalose and sucrose. Trehalose is most effective also in protecting isolated *in vitro* biostructures. In an attempt to clarify the molecular mechanisms of disaccharide bioprotection, we compared the structure and dynamics of sucrose and trehalose matrices at different hydration levels by means of high-field W-band EPR and FTIR spectroscopy. The hydration state of the samples was characterized by FTIR spectroscopy and the structural organization was probed by EPR using a nitroxide radical dissolved in the respective matrices. Analysis of the EPR spectra showed that the structure and dynamics of the dehydrated matrices as well as their evolution upon re-hydration differ substantially between trehalose and sucrose. The dehydrated trehalose matrix is homogeneous in terms of distribution of the residual water and spin-probe molecules. In contrast, dehydrated sucrose forms a heterogeneous matrix. It is comprised of sucrose polycrystalline clusters and several bulk water domains. The amorphous form was found only in 30% (volume) of the sucrose matrix. Re-hydration leads to a structural homogenization of the sucrose matrix, whilst in the trehalose matrix several domains develop differing in the local water/radical content and radical mobility. The molecular model of the matrices provides an explanation for the different protein–matrix dynamical coupling observed in dried ternary sucrose and trehalose matrices, and accounts for the superior efficacy of trehalose as a bioprotectant. Furthermore, for bacterial photosynthetic reaction centers it is shown that at low water content the protein–matrix coupling is modulated by the sugar/protein molar ratio in sucrose matrices only. This effect is suggested to be related to the preference for sucrose, rather than trehalose, as a bioprotective disaccharide in some anhydrobiotic organisms.

Introduction

Several organisms (plants, insects and microorganisms) are able to withstand for long periods (years) severe environmental conditions, such as very low or high temperatures and extreme dehydration, by entering a state called *anhydrobiosis* or *cryptobiosis*, in which their metabolic activity is essentially suspended.[1] Under such harsh environmental conditions, anhydrobiotic organisms accumulate large amounts of disaccharides, mostly sucrose and trehalose, which have been recognized to play a critical role in biopreservation through their interaction with tissues, cells, membranes and protein complexes.[2] Sucrose is mostly found in higher plants, while trehalose appears to be common among animals, lower plants and microorganisms.[1] An impressive example of the *in vivo* bioprotective action of disaccharides is provided by the largest multicellular anhydrobiotic animal, the chironomid *Polypedilum vanderplanki*, occurring in Nigeria and Uganda. Its larvae grow in temporary pools of water that frequently dry out during the lifetime of the larvae. In the dehydrated state the larvae can survive temperatures from −270 °C up to +102 °C.[3] They also tolerate high levels of gamma-ray exposure. *Polypedilum vanderplanki* has recently been shown to survive extreme drought by replacing its normal intracellular medium with a biological glass containing trehalose of up to 18% of its dry body weight.[4]

[a] *Laboratorio di Biochimica e Biofisica, Dipartimento di Farmacia e Biotecnologie, FaBiT, Università di Bologna, via Irnerio 42, I-40126 Bologna, Italy*
[b] *Max-Planck-Institut für Chemische Energiekonversion, Stiftstr. 34-36, D-45470 Mülheim (Ruhr), Germany. E-mail: anton.savitsky@cec.mpg.de; Fax: +49-208-3063951; Tel: +49-208-3063555*
[c] *Consorzio Nazionale Interuniversitario per le Scienze Fisiche della Materia (CNISM), c/o Dipartimento di Fisica, Università di Bologna, via Irnerio 46, I-40126 Bologna, Italy*
[d] *Fachbereich Physik, Freie Universität Berlin, Arnimallee 14, D-14195 Berlin, Germany*

Trehalose exhibits a multitude of different phases,[5] including various crystalline states such as the dehydrated and the α- and β-anhydrous phases, the hydrated amorphous phase and the anhydrous melt as well as the amorphous glass with moisture-dependent glass-transition temperature, T_g, which for trehalose is the highest of all disaccharides.[6] The bioprotective activity of trehalose has been postulated to be in part related to the high T_g value[6] as well as to the ability of solid trehalose to exist in more than one amorphous form or crystal structure (polymorphism).[7]

Amorphous matrices of disaccharides have received a wide interest also in view of their effectiveness in protecting isolated *in vitro* biostructures, such as enzymes[8,9] and membranes,[10] a property of substantial relevance in pharmaceutical, biotechnological and biomedical applications. To mention a few applications: an increasing number of therapeutic proteins are becoming available, often unstable in solution, which can be conveniently conserved at elevated temperature in solid amorphous disaccharide matrices after freeze-drying.[11] Among disaccharides, trehalose appears to be the most effective in stabilizing biostructures.[6] Its potentialities in providing long-term, room temperature stability to vaccines[12] and immunoconjugates[13] have been pointed out in the literature.

Despite the large attention devoted to the anhydrobiosis and biopreservation phenomena, the molecular mechanisms are still unclear, and particularly elusive is the molecular basis of the peculiar efficacy of trehalose. Extensive experimental work, exploiting neutron scattering,[14,15] Raman,[16] optical laser-flash,[17] FTIR,[18] and EPR[19] spectroscopy on different proteins incorporated into trehalose glasses, has revealed a tight protein–matrix dynamic coupling at low water content, implying that the protein conformational dynamics is controlled by that of the water–trehalose matrix.[20] FTIR studies on carboxy-myoglobin (MbCO) embedded in water–saccharide amorphous matrices have provided evidence of a tighter protein–matrix coupling to trehalose than to sucrose and other sugars.[21,22] A larger difference in the protein–matrix coupling of trehalose- and sucrose-based systems has been inferred from optical laser-flash spectroscopy in the case of a large membrane protein (a bacterial photosynthetic reaction center) for which sucrose, in contrast to trehalose, was found to be essentially unable to block the protein conformational relaxation on the time scale of 10^{-3} s, and scarcely effective in preventing protein denaturation at high temperature.[17]

The results of molecular dynamics (MD) simulations performed on MbCO[23] and lysozyme[24] embedded into a concentrated trehalose–water system further supported a strong protein–matrix dynamical coupling arising from protein–water–sugar H-bond networks. Interestingly, the dynamics of MbCO was found to be less inhibited in sucrose as compared to trehalose systems of comparable water content.[25] Recent differential scanning calorimetry studies[26,27] indicate that the denaturation temperature of several different proteins in trehalose–water matrices increases linearly with the glass transition temperature of the protein–water–sugar system, suggesting a correlation between protein unfolding and structural relaxation of the matrix.

This large body of studies has led to several (not mutually exclusive) hypotheses, in which different factors have been considered as predominant in determining the bioprotective effects: (i) stabilization *via* direct hydrogen-bonding between the sugar and the biostructure (*water-replacement hypothesis*),[28,29] a mechanism which appears to account well for membrane bioprotection;[10,30] (ii) entrapping of residual water molecules at the biomolecule–disaccharide interface (*water-entrapment hypothesis*);[31] (iii) increased rigidity *via* the extraordinary viscosity increase upon vitrification (*high-viscosity hypothesis*);[32] (iv) tight anchorage of the protein surface to the stiff matrix by residual water molecules, constrained at the protein–matrix interface by a network of H-bonds simultaneously connecting surface protein groups and disaccharide molecules (*anchorage hypothesis*).[17,19,33] According to the anchorage model the intimate interactions of different disaccharides with water and with the biomolecule *via* H-bonding are expected to modulate the protein–matrix dynamical coupling essential for forming functional pathways for protein action and, consequently, the effectiveness of bioprotection. It has also been pointed out that the pronounced polymorphism which characterizes both crystalline and amorphous phases of trehalose could play an important role in anhydrobiotic protection, avoiding water crystallization during dehydration–rehydration cycles.[7]

In an effort to clarify protein–water–sugar interaction a first step is evidently the structural and dynamical characterization of the simpler binary sugar–water systems. Many experimental and MD studies have been carried out on solutions of different sugars, including trehalose and sucrose. One could reasonably expect that the comparative study of the binary sugar–water systems formed by these two homologous disaccharides would reveal differences in their structural and dynamical features that are responsible for the superior bioprotective efficacy of trehalose. At the same time, such a comparative study would provide indispensable information for understanding the general mechanism of bioprotection in ternary biomolecule–water–sugar systems. Experimental findings obtained on sugar–water solutions by different methods (infrared, Raman, NMR and terahertz spectroscopy, ultrasound measurements, neutron and light scattering) indicated that (i) disaccharides (in particular trehalose) perturb strongly the tetrahedral intermolecular H-bond network of pure water;[34–36] (ii) trehalose promotes a more extended hydration than other disaccharides;[37,38] (iii) the trehalose–water system is characterized by a stronger solute–solvent interaction strength;[37,38] (iv) trehalose is more effective in slowing down the water dynamics.[39–41]

The structural and dynamical properties emerging from the above-mentioned experiments agree with the results of several molecular dynamics simulations, performed on sugar–water solutions. Most MD investigations deal with dilute systems (see ref. 42 and references therein), and only in a few cases investigations have been extended to a wide range of concentration (up to 80 wt%).[43–46] They showed that (i) disaccharide molecules reduce the population of water molecules as characterized by high coordination numbers, this effect being more significant in trehalose solutions; (ii) trehalose binds to a larger number of water molecules, and, at sufficiently high concentrations, reduces the size of water clusters more efficiently than

sucrose does; (iii) sucrose forms a larger number of intramolecular H bonds; (iv) consistent with observations (ii) and (iii), trehalose exhibits a larger flexibility than sucrose and other disaccharides; (v) trehalose–water solution is more homogeneous.

Many of the distinctive properties of trehalose have been suggested to be responsible for its marked bioprotective effectiveness against dehydration stresses and ice formation. When extrapolating from binary liquid solutions to solid amorphous matrices, these observations could provide, in principle, valuable hints for revealing the correct mechanism of bioprotection. However, except for only a few studies that focus on the activity of trehalose in solid forms (crystalline and amorphous) under different degrees of hydration,[47,48] structural and dynamical information available for solid disaccharide–water systems is much more limited than for binary liquid solutions. To the best of our knowledge, very few papers have addressed the comparison between trehalose and sucrose activities in the glassy state: enthalpy relaxation studies during isothermal aging indicated that, when extending the conclusion reached for concentrated solutions to the glassy state, the size of the cooperative matrix regions is much larger for trehalose than for sucrose.[49] Molecular dynamics simulations of trehalose–, maltose– and sucrose–water solutions revealed that trehalose is able to form larger clusters.[46] A comparative study of cross-polarization-magic-angle-spinning (CPMAS) ^{13}C NMR performed on trehalose, sucrose and lactose in the amorphous glassy state, paying particular attention to the glycosidic linkage C-atoms, has provided evidence of an enhanced trehalose molecular flexibility, suggesting that the conformational space explored by trehalose molecules in the amorphous phase is larger than that estimated for the other two sugars.[50] Finally, by using positron annihilation lifetime spectroscopy in trehalose matrices,[5] it was found that in the amorphous phase hydration increases the average intermolecular hole size, while in the crystalline trehalose dihydrate water is organized as a one-dimensional fluid in channels of fixed diameters, which allow water diffusion in and out of the crystallites, thereby acting as both a sink and a source of water at low moisture.

In the present work we aimed at reducing the gap between the information available for disaccharide liquid solutions and amorphous or glassy systems. We have explored the structure and dynamics of sucrose and trehalose glassy matrices at different hydration levels by means of high-field EPR spectroscopy (95 GHz/3.4 T) using the nitroxide radical 3-hydroxymethyl-2,2,5,5-tetramethylpyrrolin-1-oxyl as a well-established electron-spin probe that was dissolved in the matrices (Fig. 1). The methanethiosulfonate substituted derivative of this nitroxide radical, known as MTS spin label, is widely used in the site-directed spin labeling method (SDSL), which has become an extremely important branch of bio-EPR spectroscopy combined with site-specific mutagenesis techniques (see, for instance, ref. 51–57). Additionally, FTIR spectroscopy of the water combination ($\sim$5150 cm^{-1}) and association ($\sim$2130 cm^{-1}) bands has been used to characterize the hydration level of the sample and to examine intermolecular vibrational modes of water, which report on the coupling between different many-body states. All the matrices investigated in this work were prepared at room temperature, *i.e.*, the dehydration

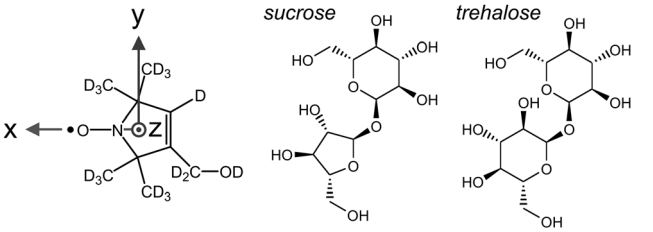

Fig. 1 Molecular structures of the perdeuterated pyrroline type nitroxide radical and of the sucrose and trehalose hosts used for diluted nitroxide binary solutions. The conventional principal axes of the *g*-tensor of the nitroxide radical are indicated.

and rehydration of the matrices was achieved only by varying the humidity level. This parameter is of particular importance for studies to understand bioprotection mechanisms.

EPR spectroscopy on nitroxide radicals, that are dissolved in a variety of matrices, can sensitively probe the physical and chemical properties of the molecular guest–host system, in particular providing information on the homogeneity or heterogeneity of the nitroxide microenvironment.[51] This information is obtained from an analysis of the nitroxide EPR spectra which provides magnetic interaction parameters as well as molecular motion parameters of the solute–solvent system. In disordered solids, in which the motion of the nitroxide guest molecules is substantially restricted, the lineshape of the EPR spectrum is governed by the following magnetic interaction parameters: (i) the dominating nitrogen electron–nuclear hyperfine interaction (characterized by the *A*-tensor components, $I(^{14}\mathrm{N}) = 1$) and (ii) the combined effect of the electron spin and orbital Zeeman interactions as well as the spin–orbit interaction (characterized by the *g*-tensor components). These interaction parameters report also on the microenvironment of the nitroxide radicals. In particular, the g_{xx} and A_{zz} principal values of the *g*- and hyperfine tensors are sensitive to the polarity and hydrogen-bonding situations of the nitroxide surrounding.[52–54] The EPR spectra are also very sensitive to the time-scales of rotational motion of the nitroxides, since such dynamics can lead to partial or even complete averaging of the magnetic interaction anisotropies.[55,56] Because of the small *g*-tensor anisotropy of nitroxide radicals the application of high-field W-band EPR methods is advantageous to ensure high orientational magneto-selectivity of the randomly distributed radicals. Moreover, high-field/high-frequency EPR excels in high spectral and high time resolutions.[55,57] Additional gain in resolution can be obtained by using perdeuterated nitroxides thereby reducing the inhomogeneous line broadening due to unresolved intramolecular proton hyperfine interactions. Furthermore, EPR spectra are sensitive to the local concentration of the spin probe and potential concentration variations in inhomogeneous solute–solvent systems. This is mainly because at higher spin concentrations the EPR lineshape is influenced by Heisenberg spin–spin exchange and dipole–dipole coupling between nearby unpaired electrons.[58] Thus, lineshape analysis allows one to learn in detail about microscopic and macroscopic heterogeneity of the guest–host system. The high-field EPR

approach, combined with a strict FTIR control of the matrix-hydration state, enabled us to develop a molecular picture of the amorphous water–sugar systems in terms of structural organization and mobility, revealing in particular the evolution of the binary system upon rehydration after dehydration. Significant structural and dynamical differences have been found between trehalose and sucrose matrices, which appear to be important for explaining the exceptional bioprotective properties of trehalose.

Experimental

Sample preparation

The molecular structure of the fully deuterated nitroxide radical (3-hydroxymethyl-2,2,5,5-tetramethylpyrrolin-1-oxyl) is shown in Fig. 1. The perdeuterated form was synthesized as described previously[59] and kindly provided by Herbert Zimmermann (Max-Planck Institute for Medical Research, Heidelberg). Sucrose (α-D-glucopyranosyl β-D-fructofuranoside) and trehalose (α-D-glucopyranosyl α-D-glucopyranoside) were purchased from Sigma-Aldrich in their highest commercially available purity and used as supplied.

The nitroxide–sucrose or –trehalose solid samples employed for FTIR measurements were obtained by starting from a 50 μL drop of an aqueous solution of 0.2 mM nitroxide, 0.835 M disaccharide, 10 mM TRIS HCl (pH 8.0) and 55 μM of the NIR dye NIR869A from QCR Solutions Corp. (Port St. Lucie, FL, USA). This drop was deposited on a CaF_2 window of 50 mm diameter and subsequently dried in a desiccator for about 5 hours under N_2 flow at room temperature. Extensive dehydration of the samples and precise control of the hydration level were achieved by using an isopiestic method as described in ref. 60. Essentially, to avoid partial or complete crystallization of the sugar matrix, following vitrification the samples were immediately exposed to a low relative humidity, r = 11%, in a gastight chamber of ~40 mL volume containing about 3 mL of an aqueous saturated LiCl salt solution. Equilibration of the samples at this relative humidity was completed in ~5 days, as judged by monitoring the water content of the samples using the area under the water combination band at ~1940 nm (see below). Rehydration of the sample was achieved by exposing, at room temperature, the matrices to saturated K_2CO_3 and NaCl aqueous solutions in order to equilibrate them at r = 43% and r = 74%, respectively.

The nitroxide–trehalose or –sucrose samples for the EPR measurements were prepared from solid matrices formed over glass plates following the procedure described above, except for omitting the NIR869A dye. The dehydrated disaccharide–nitroxide glassy matrices were crumbled into small flakes and transferred into the cylindrical sample capillaries (i.d. = 0.6 mm), made from quartz, to be inserted into the W-band EPR cavity. After the first two days of incubation at r = 11%, the solid matrices deposited on the glass plates were already dehydrated enough to enable handling, crumbling and filling of the sample capillaries as well as avoiding crystallization of the samples as a consequence of air exposure. The flakes inside the capillaries were further dehydrated by inserting a drop of saturated LiCl aqueous solution, well separated from the sample fragments. The open ends of the capillary were sealed with Critoseal (Krackeler Scientific, Inc., Albany, NY, USA), and the sample was incubated at room temperature for at least three additional days in order to achieve full equilibration at r = 11%. A similar procedure was used to obtain the rehydrated samples, except that a drop of K_2CO_3 or NaCl saturated solution was inserted inside the capillaries to obtain r = 43% or 74%, respectively.

The bacterial photosynthetic reaction center (RC) was purified from *Rhodobacter sphaeroides* R26 as described in ref. 61. The RC concentration was determined spectrophotometrically by the absorbance at 802 nm (ε_{802} = 288 mM^{-1} cm^{-1}). The ratio of the absorption at 280 to that at 800 nm was 1.3. The RC containing sugar glassy matrices, used to measure the charge recombination kinetics of the charge-separated primary donor–primary acceptor radical pair, $P_{865}^{\bullet+}Q_A^{\bullet-}$, after laser-pulse photoexcitation by transient W-band EPR, were prepared by starting from a 50 μL drop of a mixture of 0.835 M disaccharide, 10 mM TRIS HCl (pH 8.0) and LDAO 0.025% (vol/vol) and adding 168 or 56 μM RC. This protocol resulted in samples with a disaccharide/RC molar ratio of 5×10^3 or 1.5×10^4, respectively. RC–trehalose or RC–sucrose glassy samples at different hydration levels were obtained following the same procedures as described above for pure trehalose or sucrose glasses.

W-band EPR experiments

The EPR measurements were performed with a laboratory-built spectrometer operating in both cw and pulsed modes at a microwave (mw) frequency of 95 GHz (W-band) and an external magnetic field B_0 of 3.4 T.[57,62–64] For cw experiments a gold plated bronze cylindrical TE_{011} cavity was used (loaded quality factor Q_L = 2400 of the empty cavity, temperature independent in the range 90–293 K). The B_0 field was modulated at 8 kHz with an amplitude of 30 μT. To provide an absolute magnetic-field calibration and to control the sweep linearity over the desired magnetic field range a standard reference sample (Mn^{2+} in MgO) was used as a field marker.[62]

To avoid cw EPR lineshape distortions due to saturation and rapid-passage effects, the absorption and dispersion EPR responses in 0° and 90° phases relative to the modulation phase were acquired simultaneously. The mw power incident on the critically coupled loaded cavity was optimized by minimizing the integral signal component in both dispersion channels to minimize rapid-passage effects.[65–67] The 0°-dispersion signal was subjected to Hilbert transformation and, thereafter, was checked to reproduce a true absorption lineshape to exclude power-saturation effects.

The $P_{865}^{\bullet+}Q_A^{\bullet-}$ recombination kinetics data were obtained for radical pairs with thermally equilibrated spin polarization by recording their transient EPR absorption, after a laser flash, using 30 kHz field modulation and lock-in detection with 1 ms time resolution as described previously.[19]

All experimental spectra analysis and simulation procedures were performed on the basis of the EasySpin toolbox for the Matlab program package.[68,69] The $P_{865}^{\bullet+}Q_A^{\bullet-}$ recombination

kinetics was fitted to a power law by least-squares minimization routines, based on a modified Marquardt algorithm.[70] Confidence intervals of the fitting parameters were evaluated numerically as described in ref. 33 using locally developed software.

FTIR experiments

FTIR absorption measurements were performed at 297 K using a Jasco Fourier transform 6100 spectrometer, equipped with a DLATGS detector. Spectra in the mid-IR range (7000–1000 cm^{-1}) were acquired using a standard high-intensity ceramic source. Measurements were extended to the NIR region (15 000–2200 cm^{-1}) using a halogen lamp source, replacing the Ge/KBr with a Si/CaF_2 beam splitter and the KRS-5 with a CaF_2 exit interferometer window. The spectra were recorded with a resolution of 4 cm^{-1}, accumulating 10^2 or 10^3 scans per spectrum depending on the signal-to-noise ratio.

The content of residual water in the sugar matrices used in the FTIR measurements was estimated from the area under the $(\nu_2 + \nu_3)$ combination band of water around 1940 nm, essentially as described in ref. 60. The area under this band can be taken to be proportional to the water concentration, being unaffected by cosolvents, by the physical aggregation state of the sample and, in particular, by the extent of hydrogen bonding (see ref. 60 and references therein). Since the average thickness of the matrix deposited over the CaF_2 windows, *i.e.*, the effective optical path length, is not easily measured to a sufficient accuracy, we embedded a NIR dye (NIR869A) in the matrices and used the area below its absorption band (in the 700–1000 nm region) as an internal standard. In order to minimize potential perturbations due to the presence of the dye, the molar ratio (NIR869A/sugar) was kept to a minimum value equal to 5×10^{-5}. In water solutions, NIR869A has an absorption maximum at 869 nm and is characterized by an extinction coefficient of $(13.6 \pm 0.2) \times 10^3$ nm cm^{-1} mM^{-1}, as determined using a molecular weight of 841. Being sensitive to its microenvironment, upon vitrification of the sample the absorption maximum of NIR869A shifts to 930 nm, and the spectral profile undergoes slight changes. However, the spectrum is not affected by the hydration level of the solid matrices (see Fig. 2). In view of this we have determined the extinction coefficient of NIR869A in solid trehalose and sucrose samples by incorporating additionally reduced cytochrome (cyt) *c* into the matrices at a molar ratio (cyt *c*/NIR869A) = 1.5.

No changes could be detected in the spectral features of reduced cyt *c* upon incorporation into solid sugar matrices as compared to a water solution (not shown). From the peak absorbance at 550 nm, by using an extinction coefficient ε_{550} = 19.5 mM^{-1} cm^{-1}, we have determined area absorptivity coefficients for NIR869A equal to 16 770 and 13 500 nm cm^{-1} mM^{-1} in trehalose and sucrose matrices, respectively.

Results and discussion

Water quantification by FTIR

The dehydration/rehydration kinetics of the trehalose and sucrose samples have been studied by reproducing the sequence used in the EPR experiments, *i.e.*, first equilibrating the matrix at room temperature at low relative humidity (r = 11%) in the presence of a saturated aqueous LiCl solution and then exposing the sample to K_2CO_3 and NaCl vapors to set the relative humidity at r = 43% and 74%, respectively. Measurements were performed on sugar–water matrices, formed on CaF_2 windows. The matrices contained the nitroxide reporter radical at the same concentration as used in EPR experiments plus the NIR869A dye as an internal standard for the determination of the water content, as described in the Experimental section. Immediately after vitrification, before inserting the sample into the gastight holder containing the saturated LiCl solution, the trehalose and sucrose samples contained ~1.15 water per sugar molecule. During incubation in the presence of LiCl, at r = 11%, the amount of water decreased following an approximately exponential kinetics (not shown), characterized by a time constant τ of ~16 h, and reached a steady value of 0.52 and 0.41 water per sugar molecule in trehalose and sucrose, respectively. Subsequent exposition of the matrices to K_2CO_3 vapors led to steady rehydration levels with $\tau \approx 50$ h. When the samples were subsequently exposed to saturated NaCl solution a much faster rehydration occurred, resulting within about 2 h in a plasticized amorphous sample, which started to flow down on the vertical CaF_2 window. The values of the water content of both disaccharide matrices obtained by the above described procedure at the three relative humidity values are presented in Table 1. We assume that these values can be taken as a reliable estimate of water contents also for the samples used in the EPR measurements, which were rehydrated within the sample capillaries in the presence of the same standard saturated solutions.

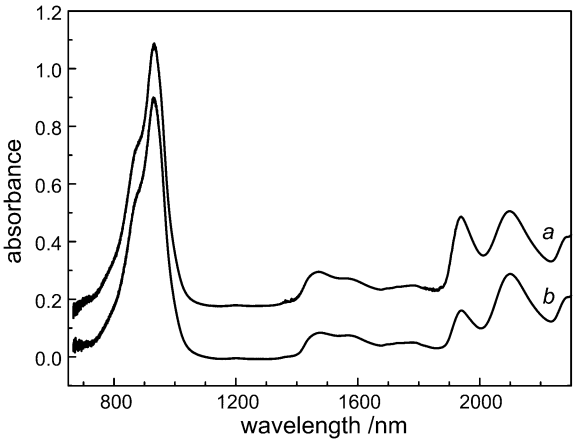

Fig. 2 NIR absorbance spectra of a NIR869A dye containing trehalose matrix equilibrated at two relative humidities: r = 74% (spectrum a), r = 11% (spectrum b). For better visual clarity the spectra have been offset by 0.2 absorbance units.

The association band of water at different hydration levels

The water association band appears in the spectrum of pure water and of hydrated binary systems in the 1800–2400 cm^{-1} range. It has been attributed to a combination of bending and librational modes,[71] *i.e.*, of modes which are extremely dependent on the molecule's microenvironment. Due to its

Table 1 Residual water content of trehalose and sucrose matrices equilibrated at different relative humidities, *r* (see text for details). Standard errors have been calculated from measurements performed on at least 5 different matrices equilibrated at the indicated *r* values

	Trehalose matrix			Sucrose matrix		
Relative humidity, *r* (%)	11	43	74	11	43	74
H_2O/sugar molar ratio	0.52 ± 0.03	0.70 ± 0.03	2.44 ± 0.06	0.41 ± 0.02	0.72 ± 0.03	2.39 ± 0.05

intermolecular character the band is particularly sensitive to the interactions of the water molecules with their neighbors. It has provided qualitative information on the structural and dynamical organization of water in several hydrated systems, including phospholipids and acylglycerols in liquid-crystalline phases,[72] protein films,[60] saccharide-coated liposomes,[73] and protein–sugar matrices.[22] In these systems, the association band generally becomes structured at low water contents, indicating that the coupling of the water bending modes with intermolecular vibrations involves also non-water H-bonding groups and, moreover, that the band can report on the diversity of the local environments experienced by the water molecules. This makes the band potentially useful when studying the structural and dynamical organization of binary trehalose– and sucrose–water systems.

Fig. 3 compares the water association bands measured in trehalose (red traces) and sucrose (black traces) matrices equilibrated at different relative humidity values *r*. The association bands recorded in pure water and in trehalose and sucrose 50% (w/w) aqueous solutions are also shown. The wavenumbers corresponding to the maxima of the bands are given in Table 2. Dehydration leads to shifts in the peak position, which are different in sucrose and trehalose, and also leads to a progressive narrowing and different structuring of the band. As a result the band profiles in trehalose and sucrose samples become significantly different upon decreasing the content of residual water.

In the most dehydrated trehalose sample, at r = 11%, the band is strongly structured exhibiting two well resolved peaks at 2134 cm^{-1} and 2062 cm^{-1}, and two marked shoulders at ~1970 cm^{-1} and 2265 cm^{-1} forming the spectral tails (bottom spectrum). The maximum at 2134 cm^{-1} is shifted towards larger wavenumbers as compared to the broad, unstructured band of pure water (Fig. 3, top spectrum) for which a maximum at 2128 cm^{-1} is found, in agreement with ref. 74. This shift is consistent with the presence of strongly H-bonded water molecules, causing an increase in the frequency of OH bending and/or librational modes. The band is similar to that measured in trehalose-dihydrate powders,[18] which show two peaks at ~2130 and 2053 cm^{-1}. The presence of these two peaks appears, therefore, to be related to water molecules which interact mostly with the sugar.[18] In the sucrose matrix the band measured at the same relative humidity (r = 11%) is significantly less structured than that in trehalose and peaks at 2119 cm^{-1}. Thus, at variance with trehalose, it exhibits a shift towards lower wavenumbers as compared to the band of pure water (Table 2).

The two sugars also differ in the evolution of the water association band upon rehydration. In the case of trehalose the

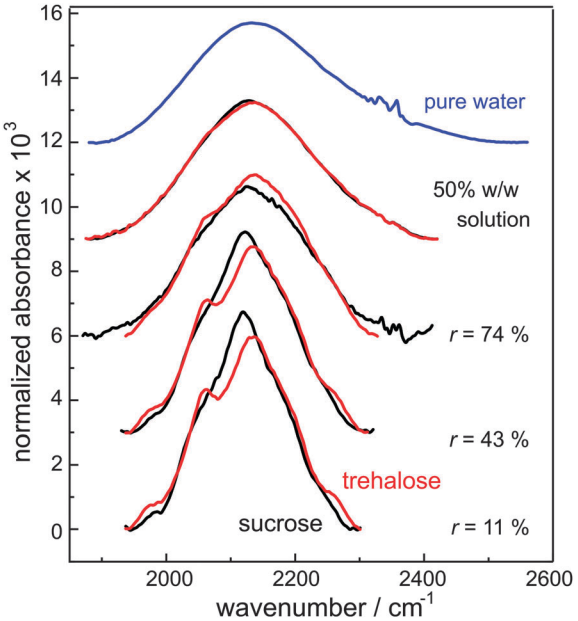

Fig. 3 Water association bands measured in trehalose (red traces) and sucrose (black traces) matrices equilibrated at different relative humidity values *r*, in the presence of saturated solutions of LiCl (r = 11%), K_2CO_3 (r = 43%) and NaCl (r = 74%). The water association bands in pure water and in trehalose and sucrose 50% w/w solutions are also shown. The bands have been normalized to unit area; the offset is done for better visual clarity.

Table 2 Spectral properties of the water association band in trehalose and sucrose systems at different hydration levels

Hydration condition	50% w/w solution	r = 74%	r = 43%	r = 11%
Trehalose peak wavenumber (cm^{-1})	2134	2134	2134	2134
Sucrose peak wavenumber (cm^{-1})	2126	2125	2122	2119
Spectra distance (SD) SD × 10^3 ($cm^{-1/2}$)	1.01	5.83	6.55	8.96

band retains a well structured character when the sample is humidified at r = 43%, and the component at ~2062 cm^{-1} is still detectable as a shoulder even at r = 74%. Interestingly, upon rehydration of the trehalose matrix (r = 43%, r = 74%), and even in the 50% (w/w) solution, the band maximum remains at 2134 cm^{-1}, *i.e.*, is shifted to higher wavenumbers as compared to pure water (Table 2). This behaviour is consistent with the larger propensity of trehalose to develop strong hydrogen bonds with water molecules, thereby forming an essentially homogeneous matrix over the whole hydration range examined here. The clearly structured band, which is observable also under hydrated conditions as high as r = 74%,

suggests that within the water–trehalose matrix a well defined and limited ensemble of H-bonded configurations is selected. At variance with this, in the sucrose matrix, rehydration progressively leads to shifts of the peak wavenumber (ν_p) towards the value of pure water (see Table 2) and to a more pronounced overall broadening of the band (see Fig. 3). In the 50% w/w sucrose solution ν_p = 2126 cm^{-1} is very close to the value observed in pure water.

It is noteworthy that the spectral features described above and their evolution with the degree of dehydration result in a progressively increasing difference between the profile of the association band in trehalose and sucrose samples upon dehydration. This behaviour, qualitatively evident in Fig. 3, can be quantitatively described by evaluating, for each hydration level, the spectra distance (SD) between the trehalose and sucrose band, defined as in ref. 18:

$$\mathrm{SD} = \left\{ \int_{\nu} \left[A^{t}(\nu) - A^{s}(\nu) \right]^{2} \mathrm{d}\nu \right\}^{1/2} \cong \left\{ \sum_{\nu} \left[A^{t}(\nu) - A^{s}(\nu) \right]^{2} \Delta\nu \right\}^{1/2} \quad (1)$$

where $A^{t}(\nu)$ and $A^{s}(\nu)$ are the normalized absorbances of the trehalose (t) and sucrose (s) samples measured at wavenumber ν, and $\Delta\nu$ is the wavenumber resolution. The values obtained for the different hydration levels (see Table 2) indicate that SD increases markedly when comparing the amorphous matrices equilibrated at r = 74% with the 50% w/w solutions. Interestingly, a significantly larger increase in SD is observed when dehydrating from r = 43% to r = 11%, than from r = 74% to r = 43% (Table 2), notwithstanding the much larger variation of the content of residual water in the latter case (*cf.* Table 1).

On the whole, the comparison of the water association band at different hydration levels indicates that different water–sugar and possibly water–water interactions take place in trehalose and sucrose samples. Particularly the increase of SD when proceeding from r = 43% to r = 11% suggests a significantly different structural organization of the sugar and residual water molecules in the trehalose and sucrose matrices at low hydration levels.

W-band EPR of dehydrated matrices

Fig. 4a shows room-temperature (RT) W-band cw EPR spectra of perdeuterated nitroxide radicals incorporated into the matrices of sucrose and trehalose, which were equilibrated to a relative humidity of r = 11% by means of a saturated LiCl solution. The nitroxide EPR spectrum in trehalose exhibits the typical powder-pattern lineshape expected for a dilute homogeneous distribution of immobilized nitroxide radicals at high magnetic fields (see Fig. 4a, lower trace). The spectrum is clearly resolved into three separate B_0 regions corresponding to the principal values of the g-tensor, *i.e.*, g_{xx}, g_{yy} and g_{zz}. Additionally, the nitrogen ^{14}N hyperfine splitting into line triplets, $I(^{14}\mathrm{N})$ = 1, is clearly observed in the g_{yy} and g_{zz} regions providing, for example, the large A_{zz} coupling. The spectrum is satisfactorily simulated using a single set of magnetic interaction parameters, g_{ii} and A_{ii}, showing that the nitroxides are exposed to a nearly homogeneous microenvironment. A multi-parameter fit of the theoretical spectrum to the experimental one, as obtained from a numerical solution of the spin Hamiltonian containing also nuclear Zeeman and quadrupole terms, yields g- and A-tensor principal values of g = [2.0082; 2.0060; 2.0024] and A = [0.58; 0.58; 3.75] mT, respectively. The error margins of the given parameter values are less than the last digit.

The EPR spectrum in the sucrose matrix differs significantly from that in the trehalose matrix. It is dominated by the single Lorentzian-shaped line (width $\Delta B_{1/2}$ = 1.0 mT) centered at g = 2.0055. This is the isotropic g-value of the nitroxide radical in the trehalose matrix. A second spectral contribution with g_{xx}, g_{zz}, and A_{zz} values identical to those of the EPR spectrum in trehalose is also observed (see Fig. 4a). Subtraction of properly

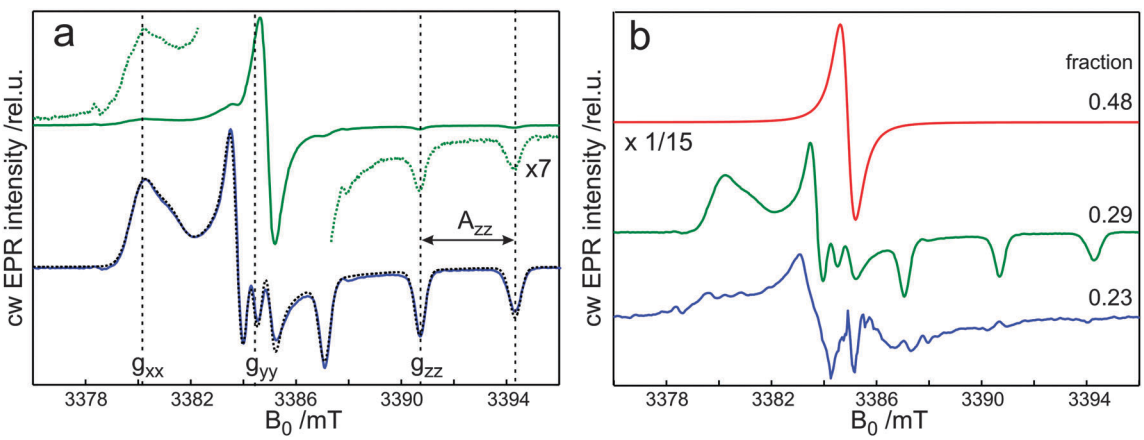

Fig. 4 (a) W-band cw EPR spectra of the perdeuterated nitroxide radical in dry sucrose (upper green trace) and trehalose (lower blue trace) matrices equilibrated at r = 11% by saturated aqueous LiCl solution. The EPR measurements were done at 293 K. The field positions corresponding to the g_{xx}-, g_{yy}- and g_{zz}-values are indicated by vertical dashed lines. The dotted traces around the upper trace are the blow-ups scaled by a factor of 7. The dotted trace overlaid with the lower trace depicts the best-fit spectrum obtained from a numerical solution of the spin Hamiltonian. (b) Deconvolution results of the W-band cw EPR spectrum of the nitroxide radical in dehydrated sucrose solution. The relative integral weights of the deconvoluted EPR spectra of three different nitroxide fractions are given at the respective spectra. Note the scaling factor (×1/15) of the upper trace.

weighted first and second contributions from the experimental EPR spectrum reveals a third spectral contribution, which is depicted in Fig. 4b. Thus, the W-band cw EPR spectrum of the nitroxide radicals in sucrose discloses at least three contributions stemming from radical fractions exposed to distinctly different microenvironments. The single Lorentzian line centered at g = 2.0055 originates in the fraction with very high local radical concentration. The high spin concentration leads to an averaging of both isotropic and anisotropic interaction parameters due to strong Heisenberg spin-exchange between and dipolar coupling of the nitroxide molecules. The second and third fractions are assigned to diluted nitroxide-matrix systems which differ in their motional dynamics. The second fraction of nitroxides is substantially restricted in the dynamics analogous to nitroxides in the trehalose matrix. The EPR spectrum of the third fraction, however, reflects that the nitroxide molecules have retained considerable rotational mobility.

In order to validate the above interpretation, the same samples were examined at a temperature well below the glass-transition temperature of water. The EPR spectrum of the trehalose sample at 150 K does not undergo any substantial changes with respect to the 293 K spectrum (see Fig. 5a, lower trace). The principal g- and A-tensor values of g = [2.0083; 2.0060; 2.0022] and A = [0.54; 0.54; 3.79] mT differ slightly from the room-temperature values. This deviation is probably due to the restriction of the nitroxide librational motion[75] and a reduced out-of-plane motion of the nitroxide oxygen[76] at 150 K as compared to that at room temperature. The g- and A-tensor values are in good agreement with those obtained previously for the same nitroxide spin probe in frozen glycerol solution at 180 K.[59] This shows the close similarity of both matrices in terms of polarity and proticity of the nitroxide microenvironments.

The 150 K cw EPR spectrum of the sucrose sample differs significantly from the room-temperature one (see Fig. 5a, upper trace). The EPR intensities are still dominated by the Lorentzian-shaped line positioned at g = 2.0055. However, the line is slightly broader ($\Delta B_{1/2}$ = 1.5 mT), and its integral intensity contribution to the overall EPR spectrum reduces from 0.48 to 0.25 when compared to the room-temperature spectrum (see Fig. 4b). The residual EPR intensity fraction of weight 0.75 can be disentangled to two contributions (not shown), one from a fraction of 0.48 with an EPR spectrum similar to that of trehalose, and another from a fraction of 0.27 with an EPR spectral shape characteristic for nitroxide radicals in frozen solution for which the lineshape is significantly influenced by dipole–dipole interaction between the radical spins. The spectral changes can be rationalized by considering the effect of restricted motional dynamics of the nitroxides that becomes allowed at room temperature (see below). Thus, the diluted fractions of the nitroxide radicals (see Fig. 4b, middle and lower traces) exhibit nearly identical EPR spectra at low temperature. The single high-concentration fraction, the EPR spectrum of which is narrowed by Heisenberg spin-exchange and rapidly fluctuating dipole–dipole interactions at room temperature, transforms into different fractions revealing a pronounced distribution of different local nitroxide concentrations within the sample volume. This results in EPR spectra showing the characteristic features of the spin-exchange narrowed regime (very high radical concentration) to the dipole-broadened regime (moderately high radical concentration).

W-band EPR of rehydrated matrices

Surprisingly, the nitroxides included in the rehydrated trehalose matrix show significantly higher mobility when compared to that observed in the sucrose matrix. To rationalize this difference, the EPR spectra were analyzed in detail using well-established algorithms. The motion of the nitroxide is strongly influenced by the dynamics and local structure of its surrounding. EPR is sensitive to rotational diffusion rather than to translational motion, since only angular motions relative to the direction of the external magnetic field B_0 affect the anisotropic magnetic interactions and, therefore, the spectral lineshapes. For isotropic Brownian

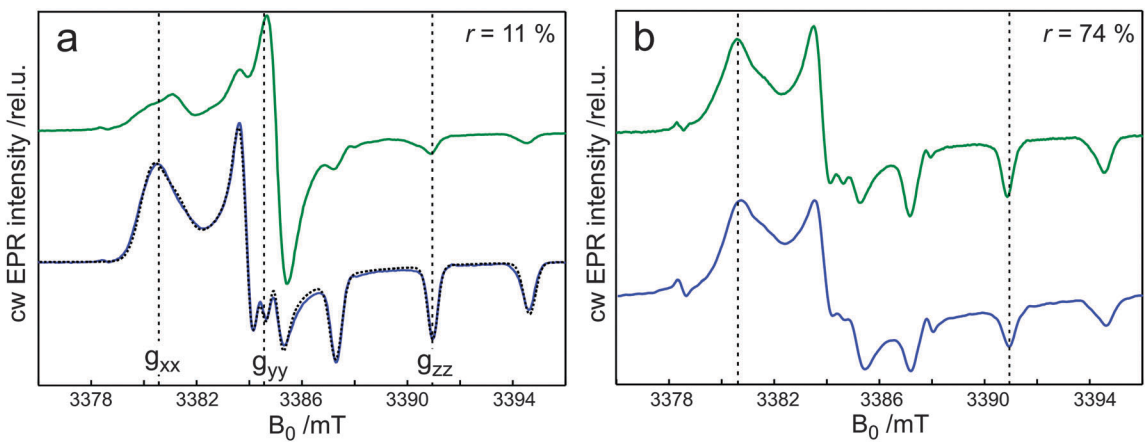

Fig. 5 W-band cw EPR spectra of the perdeuterated nitroxide radical in sucrose (upper traces) and trehalose (lower traces) matrices equilibrated at (a) r = 11% and (b) r = 74% by saturated LiCl and NaCl aqueous solutions. The EPR measurements were performed at 150 K. The field positions corresponding to the g_{xx}-, g_{yy}- and g_{zz}-values are indicated by dashed lines. The dotted trace overlaid with the lower trace in (a) depicts the best-fit EPR spectrum obtained from a numerical solution of the spin Hamiltonian.

rotational motion, the molecular dynamics is characterized by the rotational correlation time, τ_c, which is related to the rotational diffusion coefficient, D_R, by $\tau_c = (6D_R)^{-1}$. The EPR lineshape is determined by the magnitude of τ_c in relation to the magnitude of the orientation-dependent part $\Delta\omega$ of the spin Hamiltonian. $\Delta\omega$ is determined by the cumulative effect of *g*- and *A*-tensor anisotropies at high B_0 fields. At very long correlation times, $\tau_c \cdot \Delta\omega \gg 1$, a static distribution of all the possible probe orientations, *i.e.*, the rigid-limit spectrum, is observed. At very short correlation times, the spectrum approaches the fast-motion limit, $\tau_c \cdot \Delta\omega \ll 1$, and one observes only the isotropic average of the magnetic interactions. When $\tau_c \cdot \Delta\omega \approx 1$, the motion occurs within the slow-motional regime, and intermediate EPR lineshapes are observed.

The room-temperature W-band cw EPR spectra of the nitroxide-containing dry trehalose and sucrose matrices, which have been rehydrated in a controlled way at different relative humidities, are shown in Fig. 6. Upon rehydration spectra undergo distinct changes, which differ in the two sugar matrices (see Fig. 6a and b). The nitroxide EPR spectrum of the trehalose sample, rehydrated at r = 43% (K_2CO_3), mirrors the loss of matrix homogeneity. Several distinctly different nitroxide–matrix fractions, showing restricted (rigid-limit regime) and enhanced (slow-motion regime) radical mobility, are recognizable from the deconvoluted EPR spectrum. A further increase of the matrix water content (r = 74%) results in an EPR spectrum which is characteristic for nitroxide radicals in the motional-narrowing regime (see Fig. 6a, lower trace), for instance in liquid solutions.[56] Additionally, an immobilized nitroxide-matrix fraction (weight factor 0.15) is evaluated from the EPR spectrum.

The single spectral line, which dominates the EPR spectrum of the dehydrated sucrose sample, disappears completely in the sample rehydrated by the K_2CO_3 solution (r = 43%). Instead, mainly two EPR spectral contributions are observed, which correspond to immobilized (rigid limit) and still mobile (slow motion) nitroxide radicals (see Fig. 6b, middle trace). Rehydration of the sample at r = 74% results in an EPR spectrum typical for nitroxides in the slow-motion regime. The spectral contribution of the immobilized fraction is quantified to be below 10%. It should be noted that, in principle, for both sugars this immobilized fraction might stem from an incomplete rehydration of the matrices within the narrow EPR capillaries when following our rehydration protocol (see Experimental). However, re-examination of the same samples after several weeks did not reveal any significant changes of their EPR spectra showing that this fraction is indeed characteristic for both matrices.

Fig. 7a (lower trace) shows the W-band EPR spectrum of the nitroxide radicals in pure water at 293 K. The spectrum clearly shows the fast regime of the nitroxide rotational motion. A multi-parameter fit of the theoretical spectrum to the experimental one, using the fast-motion algorithm implemented in the Easy-Spin program package with the principal *g*- and *A*-tensor values obtained from the dehydrated trehalose sample at 150 K, yields τ_c = 23 ± 2 ps. This value is in good agreement with previously reported correlation times for different nitroxides in water solution at room temperature.[77]

Using the results for the water solution, the EPR spectrum of the rehydrated trehalose sample was analyzed by simulation. However, when using the best-fit value of τ_c = 350 ± 50 ps, the simulation does not reproduce the experimental spectrum very well (see Fig. 7a, middle trace). This discrepancy is likely to be due to the heterogeneity of the motional regimes of the nitroxides over the sample. In pure water solutions, the radicals are expected to have a narrow distribution of correlation times, *i.e.*, the solution is microscopically homogeneous. In contrast, in the trehalose matrix each nitroxide performs rotations in accordance with its local microenvironment, which is generally determined by the water-to-trehalose ratio. In the case of different water-to-trehalose ratios over the sample, an exact calculation of the EPR spectrum would require the local distribution of correlation times to be taken into account. Our neglect of such a distribution would explain the differences between calculated and experimental spectra.

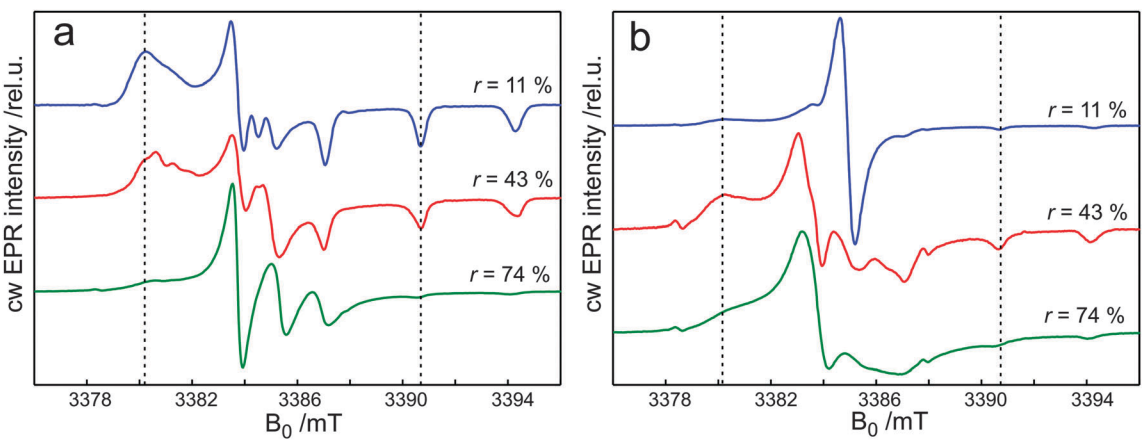

Fig. 6 Room-temperature W-band cw EPR spectra of the perdeuterated nitroxide radical in (a) trehalose and (b) sucrose matrices equilibrated at r = 11%, 43% and 74% by saturated aqueous LiCl, K_2CO_3 and NaCl solutions, respectively. The field positions corresponding to the g_{xx}- and g_{zz}-values are indicated by vertical dashed lines.

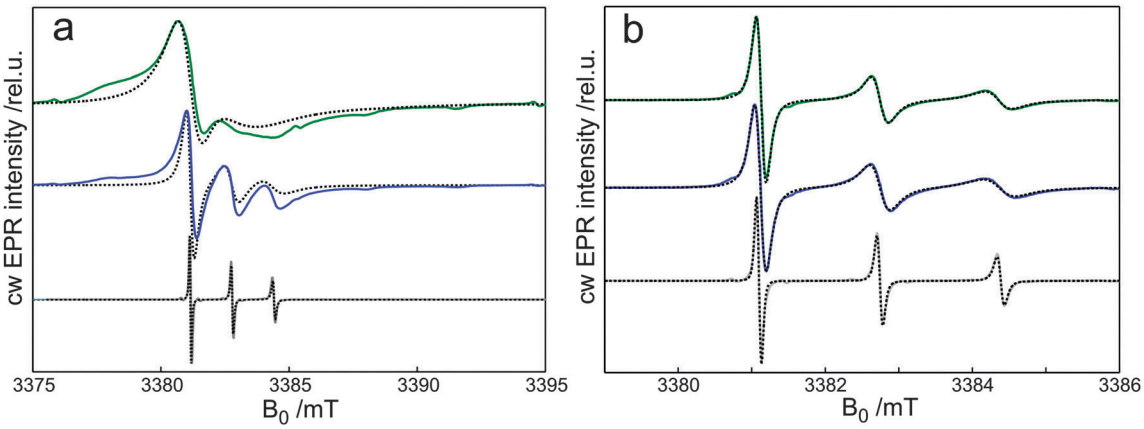

Fig. 7 (a) W-band cw EPR spectra of nitroxide radicals in water solution (lower trace), trehalose (middle trace) and sucrose (upper trace) matrices equilibrated at 74% relative humidity at 293 K. (b) W-band cw EPR spectra of 1 mM nitroxide in water (lower trace), trehalose–water 50% w/w (middle trace) and sucrose–water 50% w/w solutions (upper trace) at 293 K. The dashed lines show the calculated EPR spectra assuming isotropic rotational motion of the nitroxide molecules. For details, see text.

A similar situation is observed for the sucrose matrix (see Fig. 7a upper trace). The characteristic rotational correlation time of 1.2 ± 0.2 ns, which is obtained when using both fast- and slow-motion algorithms to describe the crossing-over between these motional regimes, is more than a factor of 3 higher than for the trehalose-matrix case, thus indicating a significantly higher microscopic viscosity in sucrose. This result is in apparent contradiction to characteristic properties of the two sugars: owing to its stronger capability to form hydrogen-bond networks the trehalose matrix is expected to have a higher microviscosity than the sucrose matrix. Fig. 7b shows W-band cw EPR spectra of the nitroxide radicals in 50% w/w water–disaccharide solutions. In such solutions the micro-environment of the radicals can be considered as homogeneous. Indeed, simulations using the fast-motion algorithm are in perfect agreement with the experimental spectra of both trehalose and sucrose (see Fig. 7b, middle and upper traces). The extracted correlation times of τ_c = 130 ± 10 ps in water–sucrose and 160 ± 10 ps in water–trehalose give a slightly higher microscopic viscosity in trehalose. This is in agreement with the results of numerous studies of water–disaccharide solutions.[78–81] The difference between τ_c = 130 ps in the 50% w/w water–sucrose solution and 1.2 ns in the rehydrated sucrose sample is reasonable considering the fact that the molar ratios of water/disaccharide are about 20 in the solution and 2.5 in the matrix, as determined by FTIR.

Because of roughly the same molar ratios for water/trehalose, the difference between τ_c = 160 ps in solution and 350 ps in the matrix is unrealistically small as long as a microscopically homogeneous hydration of the matrix is assumed. Thus, only a microscopically heterogeneous hydration with the formation of two types of domains, one domain containing predominantly only trehalose and the other domain containing trehalose–nitroxide–water, would explain the experimental observations. This explanation is also supported by examining the low-temperature EPR spectrum of the rehydrated trehalose sample (see Fig. 5b, lower trace). The positions of the g_{xx} and A_{zz} lines do not differ between the rehydrated trehalose and sucrose samples, as shown in Fig. 5b (upper trace). The lines are, however, significantly broadened in the trehalose sample. This is indicative of high local radical concentrations in the trehalose matrix, with sizable dipole–dipole interaction between the nitroxide radicals.

Model of microscopic matrix buildup

The combined results of the high-field EPR and FTIR investigations can be summarized by means of a microscopic, *i.e.*, molecular, model of the matrix structures. Fig. 8a shows a schematic representation of the dehydrated trehalose matrix. The water (0.5 per sugar molecule) and nitroxide molecules (2.4×10^{-4} per sugar molecule) are homogeneously distributed over the matrix. The nitroxide probes are well integrated into the hydrogen-bond network of water–trehalose, which restricts the guest molecule mobility allowing for only small reorientations in the librational regime. In contrast to trehalose, sucrose forms a heterogeneous matrix upon *dehydration*. At least three main types of domains can be clearly distinguished by EPR (see Fig. 8c): the first type of domains (containing 29% of overall nitroxide molecules) is similar to the trehalose matrix and includes diluted, immobilized nitroxide guests. The second type (23% of nitroxide radicals) is characterized by a higher water content, which allows for more motional freedom of the diluted guest nitroxides as compared to the first domain. The third domain type contains 48% of nitroxides in higher concentration as well as a substantial amount of water. Thus, upon dehydration, sucrose forms to a large extent crystalline clusters containing predominantly sucrose molecules. On the other hand, nitroxides and water molecules are mostly located in the interface regions between sugar clusters, both in channel (diluted nitroxides) and in bulk-water (concentrated nitroxide) domains (see Fig. 8c). Only 29% of the matrix volume consists of amorphous sucrose domains. It is noteworthy that recent small angle X-ray scattering (SAXS) measurements, performed on dehydrated sucrose matrices, have evidenced nanometric heterogeneities, attributed to the presence of sucrose nanocrystals.[82]

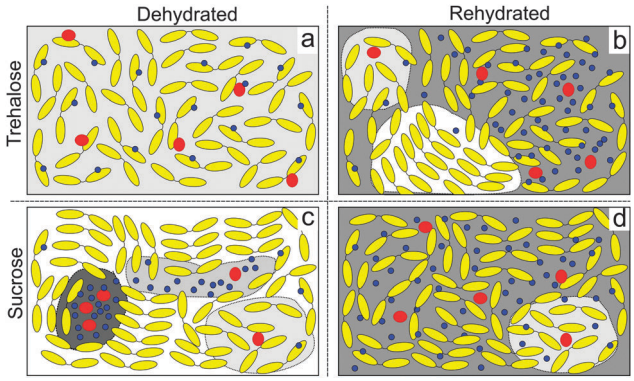

Fig. 8 Schematic 2D representation of the microscopic buildup of a macroscopic region of trehalose (top) and sucrose (bottom) matrix solutions of nitroxide spin probes for two hydration levels: (a, c) dehydrated, containing 0.5 water per sugar molecule and (b, d) rehydrated, containing 2.4 water per sugar molecule. The yellow, blue and red symbols denote sugar, water and nitroxide molecules, respectively. The filled areas mark the following states: white – polymorphic crystalline; light, medium and dark gray – amorphous state with increasing water concentrations.

Upon *rehydration*, the structures of the sucrose and trehalose matrices undergo significant changes following, however, different scenarios. In sucrose, increasing the water content to 0.7 per sugar molecule leads to complete disappearance of the bulk-water domains. This can be rationalized by considering the development of channel domains into bulk-water domains. This leads to a redistribution of the nitroxide guest molecules due to the onset of diffusion throughout the bulk and channel volumes. Further hydration (2.5 water per sugar molecule) only increases the water content of these two domain types up to an almost complete homogenization of the matrix. This allows for a homogeneous nitroxide distribution, which is characterized by a high microscopic viscosity because of the low global water concentration. In contrast, for the *trehalose* matrix the end stage of the rehydration (r = 74%) is characterized by the presence of three domain types. The first and second types, with high water content (low microscopic viscosity, very mobile nitroxides) and low water content (high microscopic viscosity, immobilized nitroxides), are directly probed by EPR. A third type of domains, which contains predominantly trehalose molecules, has to be assumed additionally. This assumption is based on combining the findings of FTIR and EPR. FTIR reveals only 2.4 water per trehalose molecule in the rehydrated trehalose matrix. The rotational mobility of the largest nitroxide fraction is, however, significantly higher compared to that of the rehydrated sucrose matrix with the same overall water content. Moreover, this mobility is slowed down by only a factor of 2 as compared to water–trehalose 50% w/w solution containing about 20 water molecules per sugar molecule. Thus, in the rehydrated trehalose matrix the water and nitroxides are predominantly located in a partial volume of the matrix and another part has to be occupied by trehalose crystalline clusters, analogous to the dehydrated sucrose matrix.

In order to test the possibility that nitroxide radicals could be included in the crystalline domains, which would shed doubt on the derived model depicted in Fig. 8, crystals of nitroxide-doped disaccharides were examined by EPR. The crystals were obtained from saturated disaccharide aqueous solutions containing 1 mM nitroxide by slowly cooling down the solutions to +4 °C. Remarkably, after purification the crystals did not reveal any nitroxide EPR signals. This observation supports our assumption that the radicals are not included in the polycrystalline domains.

Our EPR investigation cannot provide information on the size of the identified domains pictorially represented in Fig. 8. This information would be relevant to compare our results with those of computational studies on the structural and dynamical properties of sugar matrices. In particular, since simulations are generally limited to boxes which do not exceed ~10 nm in side length (see ref. 24), they may not be able to capture structural heterogeneities of the system resulting from domains of larger size. A combined approach based on small angle and ultra small angle neutron and X-ray scattering (SANS, USANS, SAXS, USAXS) appears to be most suited to evaluate the size of the detected domains, delivering in principle structural information from the nanometer to the micrometer scale.

Ternary protein–water–sugar systems

The different structural and dynamical organization of dried trehalose and sucrose matrices, as revealed at the microscopic scale by the present study, provides a reasonable explanation for the different protein–matrix dynamical coupling, which has been observed in ternary protein–water–sugar systems formed by trehalose or sucrose at low hydration levels.[17] The much tighter protein–matrix coupling occurring in trehalose is evidenced by the larger efficacy of trehalose in reducing large scale protein dynamics responsible for protein unfolding at high temperatures. The remarkable superiority of trehalose in preserving the structure and function at low water content and elevated temperature has been demonstrated for a number of soluble proteins (see ref. 8 and 9 as well as ref. 83–85 for DNA restriction and modifying enzymes). Such a behaviour is even more pronounced in the case of a large membrane protein complex like the bacterial photosynthetic reaction center (RC). Its structural and functional integrity was fully preserved for 6 days at 37 °C when incorporated into a dried trehalose matrix, while it was totally lost in 5 days when embedded in a comparably dehydrated sucrose matrix.[17]

The RC from the purple bacterium *Rhodobacter* (*Rb.*) *sphaeroides* is an excellent model system for investigating the coupling between matrix and conformational dynamics associated to its photocatalytic activity.[19,20] Following photoactivation, this pigment–protein complex catalyzes a primary charge separation event, in which a photoexcited bacteriochlorophyll "special pair" (P_{865}) delivers an electron, within ~200 ps, to a ubiquinone molecule (Q_A) located ~25 Å away from P_{865} (for reviews, see ref. 86,87). Under physiological conditions the RC protein responds to the electric field, which is generated by the charge-separated radical-pair $P_{865}^{\bullet+}Q_A^{\bullet-}$ state, by relaxing, on a time scale shorter than 10^{-3} s, from a dark-adapted to a light-adapted conformation that markedly stabilizes the $P_{865}^{\bullet+}Q_A^{\bullet-}$ state (see ref. 60 and

references therein). As shown by low-temperature studies,[88,89] this dielectric relaxation of the RC protein, as well as the thermal fluctuations of the RC between conformational substates, is sensitively probed by the kinetics of charge recombination, in which the electron directly tunnels from $Q_A^{\bullet-}$ to $P_{865}^{\bullet+}$. In fact, retardation of the conformational dynamics, by preventing $P_{865}^{\bullet+}Q_A^{\bullet-}$ stabilization and interconversion among conformational substates, results in a significantly accelerated and rate-distributed recombination kinetics. From this it was concluded that the incorporation of the RC into an increasingly dehydrated trehalose glass progressively hinders its conformational dynamics.[17,19,33,90,91] In extremely dehydrated trehalose matrices, the average rate constant, $\langle k \rangle$, which is equal to 10 s^{-1} in solutions at RT, increases up to $\langle k \rangle$ = 28 s^{-1}, and a drastic broadening of the rate distribution occurs in parallel. This behaviour, which mimics the kinetics observed in dark-adapted RCs frozen at cryogenic temperatures in water–glycerol systems, indicates that the relaxation from the dark-adapted to the light-adapted conformations as well as the substate interconversions is fully inhibited at room temperature. This is due to the tight coupling of the internal degrees of freedom of the protein to those of the embedding trehalose matrix.[90] At variance with this, in dehydrated sucrose amorphous matrices, the conformational RC dynamics, as probed by $P_{865}^{\bullet+}Q_A^{\bullet-}$ recombination, is only marginally reduced relative to that in solution, in spite of the extreme viscosity and rigidity of the embedding sucrose matrix.[17] From this it was concluded that, at variance with the trehalose situation, the dynamical coupling between the RC and the sucrose matrix is extremely weak, suggesting that, at sufficiently low water content, a protein–matrix "nanophase separation" takes place.[17] This suggestion is strongly supported by the results of the present EPR study, which have revealed a strong matrix heterogeneity in dehydrated (r = 11%) binary sucrose–water systems. While in the trehalose glass of comparably low hydration the nitroxide probes appear homogeneously distributed and essentially immobilized within the hydrogen bond network of the water–sugar system, in the sucrose–water matrix three different domains can be resolved on the basis of the deconvoluted nitroxide EPR spectrum: in one of these domains about 50% of the nitroxides are "nanophase separated" in the presence of residual water in the matrix (see Fig. 8). This organization clearly implies a dynamical decoupling between the guest molecule surrounded by water and the large stiff clusters of polycrystalline sucrose formed under low hydration.

The results obtained in the binary water–trehalose and water–sucrose amorphous systems at different hydration levels are in line with the *anchorage* model, which was proposed to explain the sugar-specific dynamic coupling in protein–water–sugar matrices.[17,19,33] As mentioned in the Introduction, the model assumes that, upon reducing the water content of the matrix below a threshold value, a growing fraction of the residual hydration shell of the protein becomes involved in a hydrogen-bond network that connects exposed protein groups and sugar molecules, thus locking the protein surface dynamics to the restricted dynamics of the solid matrix. This "slaving" scenario of molecular dynamics[92] is consistent with the present EPR results, which emphasize the role of specific sugar–water interactions in determining the microscopic organization of the matrix and its evolution upon dehydration, which differ strongly in trehalose and sucrose amorphous systems.

In view of the low nitroxide/sugar molar ratio used to study the binary water–sugar systems (2.4×10^{-4}, see Experimental), we expect that the spin probe does not perturb significantly the structural organization of the water–sugar matrix and, therefore, authentically reports on the genuine structural and dynamical properties of a *bulk* trehalose–water or sucrose–water matrix. In this respect it is important to recall that the above summarized studies on the RC–matrix coupling were all performed at a high sugar/protein molar ratio (10^4). Under these conditions, although some influence of the large RC protein complex on the matrix properties cannot be excluded, it seems reasonable to assume that the structural organization of the matrix is mainly dictated by the *bulk* behaviour of the sugar matrix. Therefore, the homogeneity/heterogeneity characteristics of the trehalose or sucrose matrix, as probed by the nitroxide radical at low water content, are well consistent with the degree of protein–matrix coupling or uncoupling, as probed by the $P_{865}^{\bullet+}Q_A^{\bullet-}$ recombination kinetics in RC–sugar matrices at a high sugar/protein molar ratio.

To further explore these aspects we have undertaken a systematic study of the effect of the sugar/protein molar ratio on the protein–matrix coupling using the RC from *Rb. sphaeroides* R26 as a model system. The relevance of the sugar/protein molar ratio as a parameter for governing the structural and dynamical organization of a ternary protein–water–sugar system becomes apparent from Fig. 9. It shows the charge-recombination kinetics of $P_{865}^{\bullet+}Q_A^{\bullet-}$ after laser-pulse photoexcitation, as measured by lock-in detection transient W-band EPR[19] on RCs embedded in trehalose and sucrose matrices: the samples are characterized by two sugar molar ratios, and equilibrated at two selected values of relative humidity.

In RC–trehalose matrices characterized by a high sugar/RC molar ratio (1.5×10^4) dehydration of the sample (from r = 74% to r = 11%) results in a substantial acceleration of the kinetics, which becomes also significantly more distributed in rate (Fig. 9a). As already reported,[19,33,90] the kinetic traces, $N(t)$, normalized to the amplitude $N(0)$ at the time of the laser flash (t = 0), are well fitted to a power law

$$N(t)/N(0) = (1 + \lambda \times t)^{-n} \quad (2)$$

with the parameters λ and n related to the average decay rate constant $\langle k \rangle = n \times \lambda$ and to the variance of the rate distribution function $\sigma^2 = n \times \lambda^2$. The results of the fit are summarized in Table 3.

In RC–sucrose matrices, on the other hand, which are characterized by the same high sugar/RC molar ratio, the same extent of dehydration (from r = 74% to r = 11%) does not accelerate the kinetics, and has only a limited effect on σ (Fig. 9b and Table 3). These results fully agree with what was observed in trehalose and sucrose matrices at a molar ratio of

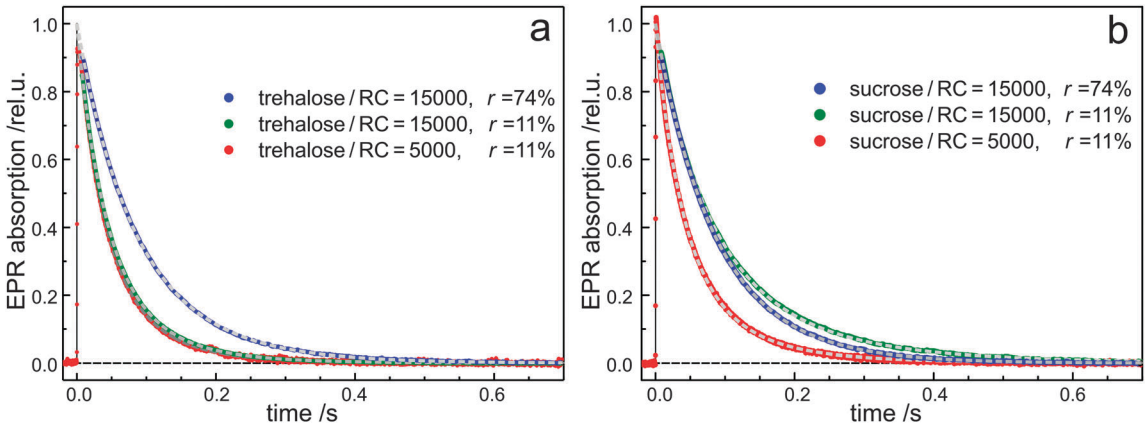

Fig. 9 Kinetics of $P_{865}^{\bullet+}Q_A^{\bullet-}$ recombination measured by transient W-band EPR following a 532 nm laser pulse in RCs embedded in trehalose (a) and sucrose (b) matrices at room temperature. The traces were acquired at the maximum EPR absorption of the thermally equilibrated $P_{865}^{\bullet+}$ cofactor, as described previously.[19] The samples are characterized by a different sugar/RC molar ratio, and equilibrated at a relative humidity r = 74% and 11%, respectively. Fitting the signals to a power law[33] (grey continuous lines) yields the values of the average rate constant, $\langle k \rangle$, and of the rate distribution width, σ, which are given in Table 3.

10^4 by optical flash spectroscopy,[17] confirming the dynamical protein–matrix coupling and uncoupling typical of dehydrated trehalose and sucrose amorphous solid matrices. It is noteworthy that, when the sugar/RC molar ratio is reduced from 1.5×10^4 to 5×10^3, dehydration of the RC–sucrose matrix results in accelerated and rate-distributed $P_{865}^{\bullet+}Q_A^{\bullet-}$ recombination kinetics, very similar to what is recorded in the trehalose matrix at both high (1.5×10^4) and low (5×10^3) sugar/RC molar ratios (Fig. 9 and Table 3). In other words, at variance with trehalose, the protein–matrix coupling strength in sucrose matrices appears to be strongly modulated by the sugar/protein molar ratio.

Measurements performed by optical flash absorption spectroscopy over a range of sugar/RC ratios indicate that the behaviour reported above is system-specific and that the transition from an essentially uncoupled to a coupled regime occurs progressively upon decreasing the molar ratio from 10^4 to 10^3 (Malferrari *et al.*, in preparation). Furthermore, the efficacy of sucrose matrices in impairing fast RC conformational dynamics at low sugar/protein ratios is paralleled by an increased efficacy also in protecting against thermal denaturation under dehydrated conditions (Malferrari *et al.*, in preparation). The latter observation, indicating a modulation of the protein–matrix coupling that governs large-scale protein dynamics related to unfolding, could explain why not only trehalose, but also sucrose is synthesized in large amounts by some anhydrobiotic organisms when they are exposed to adverse environmental conditions. We suggest that, at low sucrose/RC ratios, the hosted protein perturbs substantially the heterogeneous organization of the *bulk* sucrose–water matrix, which is detected in the present study at low hydration levels (see Fig. 8), thereby inhibiting in particular the protein–matrix nanophase separation. It is likely that the presence of the protein at a higher concentration in the matrix disorganizes the packing of sucrose molecules (sucrose clusters, see Fig. 8). Probably, at a high protein concentration also water–water interactions are reduced, thus limiting water mobility. This reorganization can evidently give rise to a dynamic coupling between the sucrose matrix and the protein, similar to the one taking place in trehalose matrices even at high sugar/protein molar ratios.

Conclusion

Our comparative study of the homologous disaccharides trehalose and sucrose glassy matrices is based on the detailed analysis of the W-band high-field EPR spectra of a perdeuterated nitroxide spin probe hosted in the solid sugar systems at three representative hydration states, which have been characterized by FTIR spectroscopy of the residual water. The information gained from the EPR analysis allowed us to develop a molecular model of the matrices (summarized in Fig. 8) which defines, at the mesoscopic scale,

Table 3 Kinetic parameters of the $P_{865}^{\bullet+}Q_A^{\bullet-}$ recombination process as determined from the EPR decays in trehalose and sucrose matrices, which are characterized by two different sugar/RC molar ratios (m) and are equilibrated at different relative humidities (r). The indicated errors correspond to confidence intervals within 2 standard deviations (see Experimental)

Sample	Trehalose r = 74% $m = 15 \times 10^3$	Trehalose r = 11% $m = 15 \times 10^3$	Trehalose r = 11% $m = 5 \times 10^3$	Sucrose r = 74% $m = 15 \times 10^3$	Sucrose r = 11% $m = 15 \times 10^3$	Sucrose r = 11% $m = 5 \times 10^3$
$\langle k \rangle$ (s^{-1})	11.73 ± 0.02	21.92 ± 0.03	23.63 ± 0.11	11.76 ± 0.02	11.88 ± 0.04	22.68 ± 0.11
σ (s^{-1})	3.12 ± 0.03	9.20 ± 0.03	9.87 ± 0.14	2.65 ± 0.03	5.14 ± 0.06	10.88 ± 0.17

important dynamical and structural features of the two systems. We have found that trehalose and sucrose give rise to amorphous/polycrystalline matrices which exhibit under severe dehydration a strikingly different structural organization and quite distinct dynamic regimes. Trehalose forms a homogeneous amorphous phase in which the hosted nitroxide molecules are uniformly distributed; their rotational mobility at room temperature is dramatically impaired, to an extent comparable to that observed in the same matrices at 150 K. In contrast, at a comparable degree of dehydration sucrose forms a highly heterogeneous phase characterized by the presence of extended crystalline sugar clusters that are essentially deprived of water and nitroxide molecules. The solute nitroxide is mostly concentrated in the water-rich domains and, to a lesser extent, dispersed in channels connecting the bulk-water domains. In the latter two aqueous microenvironments the hosted probe molecule maintains a significant motional freedom, in spite of the large overall macroviscosity of the system. Only 30% of the nitroxide probe is immobilized in the sucrose matrix, similar to what happens in the trehalose matrix, and defines an additional matrix domain. Interestingly, the evolution of the structural organization of the system upon rehydration also differs in the trehalose and sucrose matrices. A moderate increase in the content of residual water, from 0.4 to 0.7 water per sugar molecule, destroys the bulk-water domains. In the sucrose matrix, upon further rehydration up to 2.5 water per sucrose molecule, an essentially homogeneous phase is obtained. In the trehalose matrix, on the other hand, a corresponding level of rehydration leads to a heterogeneous redistribution of the water molecules, resulting in two different domains. They are characterized by either low or high water content, in which the nitroxide probes are still immobilized or highly mobile, respectively.

The molecular picture obtained for binary disaccharide–water systems is of great help in clarifying the mechanisms by which disaccharide matrices restrict, in ternary systems, the dynamics of hosted biomolecules, *e.g.*, protein complexes. First of all, the immobilization of the nitroxide probe in trehalose matrices of very low water content, for which the extent of immobilization is comparable at room temperature and 150 K, accounts for the ability of trehalose matrices to reduce at room temperature the dynamics of matrix-embedded proteins to levels observable only at cryogenic temperature in the hydrated system.[14,20,90] From the present observations, when considering the structural and dynamic homogeneity of the dehydrated trehalose matrix, we infer the formation of an H-bond network, involving the water and trehalose molecules, which extends homogeneously over the whole matrix and which is able to integrate and immobilize the hosted nitroxide probe as well. Such a multiple, extended H-bond network has been proposed earlier to explain the tight protein–matrix dynamical coupling in dehydrated ternary trehalose systems with embedded photosynthetic RCs[17] (*anchorage hypothesis*).[20]

The results of the present study further clarify the mechanisms of protein–matrix interaction by providing, most importantly, a reasonable explanation for the superior efficacy of trehalose, as compared to sucrose, in inhibiting the dynamics of matrix-embedded proteins, thus determining the extraordinary bioprotective properties of trehalose. We found that, in contrast to trehalose, the dehydrated sucrose matrix is strongly heterogeneous, being mostly formed by sugar polycrystalline domains, which exclude the guest molecule, and bulk-water domains that are connected by water channels. They allow for a significant mobility of the embedded guest molecule. Therefore, the structural heterogeneity of the dehydrated sucrose matrix, which develops upon strong dehydration, appears to be responsible for the inability to significantly retard the dynamics of the hosted biomolecules, in spite of the extremely high macroviscosity of the system. A particularly pronounced protein/matrix dynamical uncoupling was observed earlier in dehydrated sucrose matrices embedding photosynthetic RCs[17] and was proposed to arise from a nanophase separation occurring in the ternary system upon dehydration. This conclusion is strongly supported by the results of the present study for dehydrated binary sucrose systems. Since the above-mentioned RC–trehalose matrices[17] were characterized by a large (10^4) sugar/protein molar ratio, their structural organization can be assumed to be mainly governed by the behaviour of the bulk trehalose matrix, which becomes strongly homogeneous upon dehydration.

It is not surprising that, as shown in the last section of the present work for RC–sucrose matrices, the dynamical protein–matrix coupling/decoupling depends critically upon the protein concentration in the embedding matrix. Our analysis of the binary disaccharide systems suggests, in fact, that the complex structural organization of the matrix is the result of a subtle interplay between water–water, water–sugar, and sugar–sugar interactions. These multi-body interactions which determine, in the dehydrated pure sucrose matrix, a highly heterogeneous structural organization and microdynamics, are likely to be strongly perturbed in the ternary system at sufficiently high protein concentrations, giving rise to a significant protein–matrix dynamical coupling. The observation that the protein–matrix coupling is not only sugar-specific, but can also be additionally modulated by the sugar/protein ratio might be relevant to understand why not only trehalose, but also other homologous disaccharides, in particular sucrose, appear to be involved in the biopreservation of anhydrobiotic organisms. We expect that direct information on the structural and dynamical organization of protein–water–sucrose amorphous systems, as a function of the protein concentration, can be obtained by extending the high-field EPR approach to ternary RC–water–sucrose systems that include a nitroxide spin probe. Experiments along this line are under way in our laboratories.

Acknowledgements

We gratefully acknowledge financial support by the Cluster of Excellence RESOLV (EXC 1069) funded by the Deutsche Forschungsgemeinschaft and the Max-Planck-Gesellschaft. The financial support of MIUR of Italy is acknowledged by M.M., F.F. and G.V. G.V. thanks L. Cordone (Palermo University) for stimulating discussions.

References

1 J. S. Clegg, Cryptobiosis - a Peculiar State of Biological Organization, *Comp. Biochem. Physiol., Part B: Biochem. Mol. Biol.*, 2001, **128**, 613–624.

2 L. M. Crowe, Lessons from Nature: The Role of Sugars in Anhydrobiosis, *Comp. Biochem. Physiol., Part A: Mol. Integr. Physiol.*, 2002, **131**, 505–513.

3 H. E. Hinton, Fly Larva that Tolerates Dehydration and Temperatures of −270 °C to +102 °C, *Nature*, 1960, **188**, 336–337.

4 M. Sakurai, T. Furuki, K.-i. Akao, D. Tanaka, Y. Nakahara, T. Kikawada, M. Watanabe and T. Okuda, Vitrification is Essential for Anhydrobiosis in an African Chironomid, Polypedilum Vanderplanki, *Proc. Natl. Acad. Sci. U. S. A.*, 2008, **105**, 5093–5098.

5 D. Kilburn, S. Townrow, V. Meunier, R. Richardson, A. Alam and J. Ubbink, Organization and Mobility of Water in Amorphous and Crystalline Trehalose, *Nat. Mater.*, 2006, **5**, 632–635.

6 L. M. Crowe, D. S. Reid and J. H. Crowe, Is Trehalose Special for Preserving Dry Biomaterials?, *Biophys. J.*, 1996, **71**, 2087–2093.

7 F. Sussich, C. Skopec, J. Brady and A. Cesaro, Reversible Dehydration of Trehalose and Anhydrobiosis: From Solution State to an Exotic Crystal?, *Carbohydr. Res.*, 2001, **334**, 165–176.

8 W. Q. Sun and P. Davidson, Protein Inactivation in Amorphous Sucrose and Trehalose Matrices: Effects of Phase Separation and Crystallization, *Biochim. Biophys. Acta*, 1998, **1425**, 235–244.

9 E. C. López-Díez and S. Bone, The Interaction of Trypsin with Trehalose: An Investigation of Protein Preservation Mechanisms, *Biochim. Biophys. Acta*, 2004, **1673**, 139–148.

10 F. Albertorio, V. A. Chapa, X. Chen, A. J. Diaz and P. S. Cremer, The α,α-(1 → 1) Linkage of Trehalose is Key to Anhydrobiotic Preservation, *J. Am. Chem. Soc.*, 2007, **129**, 10567–10574.

11 W. Wang, Lyophilization and Development of Solid Protein Pharmaceuticals, *Int. J. Pharm.*, 2000, **203**, 1–60.

12 H. J. Choi, D. G. Yoo, B. J. Bondy, F. S. Quan, R. W. Compans, S. M. Kang and M. R. Prausnitz, Stability of Influenza Vaccine Coated onto Microneedles, *Biomaterials*, 2012, **33**, 3756–3769.

13 C. Selva, M. Malferrari, R. Ballardini, A. Ventola, F. Francia and G. Venturoli, Trehalose Preserves the Integrity of Lyophilized Phycoerythrin-Antihuman CD8 Antibody Conjugates and Enhances their Thermal Stability in Flow Cytometric Assays, *J. Pharm. Sci.*, 2013, **102**, 649–659.

14 L. Cordone, M. Ferrand, E. Vitrano and G. Zaccai, Harmonic Behaviour of Trehalose-Coated Carbon-Monoxy-Myoglobin at High Temperature, *Biophys. J.*, 1999, **76**, 1043–1047.

15 G. Caliskan, D. Mechtani, J. H. Roh, A. Kisliuk, A. P. Sokolov, S. Azzam, M. T. Cicerone, S. Lin-Gibson and I. Peral, Protein and Solvent Dynamics: How Strongly are They Coupled?, *J. Phys. Chem.*, 2004, **121**, 1978–1983.

16 G. Caliskan, A. Kisliuk, A. M. Tsai, C. L. Soles and A. P. Sokolov, Protein Dynamics in Viscous Solvents, *J. Phys. Chem.*, 2003, **118**, 4230–4236.

17 F. Francia, M. Dezi, A. Mallardi, G. Palazzo, L. Cordone and G. Venturoli, Protein-Matrix Coupling/Uncoupling In ''Dry'' Systems of Photosynthetic Reaction Center Embedded in Trehalose/Sucrose: The Origin of Trehalose Peculiarity, *J. Am. Chem. Soc.*, 2008, **130**, 10240–10246.

18 S. Giuffrida, G. Cottone, F. Librizzi and L. Cordone, Coupling between the Thermal Evolution of the Heme Pocket and the External Matrix Structure in Trehalose Coated Carboxy-myoglobin, *J. Phys. Chem. B*, 2003, **107**, 13211–13217.

19 A. Savitsky, M. Malferrari, F. Francia, G. Venturoli and K. Möbius, Bacterial Photosynthetic Reaction Centers in Trehalose Glasses: Coupling between Protein Conformational Dynamics and Electron-Transfer Kinetics as Studied by Laser-Flash and High-Field EPR Spectroscopies, *J. Phys. Chem. B*, 2010, **114**, 12729–12743.

20 L. Cordone, G. Cottone, S. Giuffrida, G. Palazzo, G. Venturoli and C. Viappiani, Internal Dynamics and Protein-Matrix Coupling in Trehalose-Coated Proteins, *Biochim. Biophys. Acta*, 2005, **1749**, 252–281.

21 S. Giuffrida, G. Cottone and L. Cordone, Structure-Dynamics Coupling Between Protein and External Matrix in Sucrose-Coated and in Trehalose-Coated MbCO: An FTIR study, *J. Phys. Chem. B*, 2004, **108**, 15415–15421.

22 S. Giuffrida, G. Cottone and L. Cordone, Role of Solvent on Protein-Matrix Coupling in MbCO Embedded in Water-Saccharide Systems: A Fourier Transform Infrared Spectroscopy Study, *Biophys. J.*, 2006, **91**, 968–980.

23 G. Cottone, L. Cordone and G. Ciccotti, Molecular Dynamics Simulation of Carboxy-Myoglobin Embedded in a Trehalose-Water Matrix, *Biophys. J.*, 2001, **80**, 931–938.

24 A. Lerbret, F. Affouard, A. Hedoux, S. Krenzlin, J. Siepmann, M.-C. Bellissent-Funel and M. Descamps, How Strongly Does Trehalose Interact with Lysozyme in the Solid State? Insights from Molecular Dynamics Simulation and Inelastic Neutron Scattering, *J. Phys. Chem. B*, 2012, **116**, 11103–11116.

25 G. Cottone, S. Giuffrida, G. Ciccotti and L. Cordone, Molecular Dynamics Simulation of Sucrose- and Trehalose-Coated Carboxy-Myoglobin, *Proteins: Struct., Funct., Bioinf.*, 2005, **59**, 291–302.

26 G. Bellavia, G. Cottone, S. Giuffrida, A. Cupane and L. Cordone, Thermal Denaturation of Myoglobin in Water-Disaccharide Matrixes: Relation with the Glass Transition of the System, *J. Phys. Chem. B*, 2009, **113**, 11543–11549.

27 G. Bellavia, S. Giuffrida, G. Cottone, A. Cupane and L. Cordone, Protein Thermal Denaturation and Matrix Glass Transition in Different Protein-Trehalose-Water Systems, *J. Phys. Chem. B*, 2011, **115**, 6340–6346.

28 J. F. Carpenter and J. H. Crowe, An Infrared Spectroscopic Study of the Interactions of Carbohydrates with Dried Proteins, *Biochemistry*, 1989, **28**, 3916–3922.

29 S. D. Allison, B. Chang, T. W. Randolph and J. F. Carpenter, Hydrogen Bonding Between Sugar and Protein is Responsible for Inhibition of Dehydration-Induced Protein Unfolding, *Arch. Biochem. Biophys.*, 1999, **365**, 289–298.

30 A. K. Sum, R. Faller and J. J. de Pablo, Molecular Simulation Study of Phospholipid Bilayers and Insights of the Interactions with Disaccharides, *Biophys. J.*, 2003, **85**, 2830–2844.

31 P. S. Belton and A. M. Gil, IR and Raman-Spectroscopic Studies of the Interaction of Trehalose with Hen Egg-White Lysozyme, *Biopolymers*, 1994, **34**, 957–961.
32 J. G. Sampedro and S. Uribe, Trehalose-Enzyme Interactions Result in Structure Stabilization and Activity Inhibition, The Role of Viscosity, *Mol. Cell. Biochem.*, 2004, **256**, 319–327.
33 F. Francia, M. Malferrari, S. Sacquin-Mora and G. Venturoli, Charge Recombination Kinetics and Protein Dynamics in Wild Type and Carotenoid-less Bacterial Reaction Centers: Studies in Trehalose Glasses, *J. Phys. Chem. B*, 2009, **113**, 10389–10398.
34 C. Branca, S. Magazu, G. Maisano and P. Migliardo, Anomalous Cryoprotective Effectiveness of Trehalose: Raman Scattering Evidences, *J. Phys. Chem.*, 1999, **111**, 281–287.
35 F. Affouard, P. Bordat, M. Descamps, A. Lerbret, S. Magazu, F. Migliardo, A. J. Ramirez-Cuesta and M. F. T. Telling, A Combined Neutron Scattering and Simulation Study on Bioprotectant Systems, *Chem. Phys.*, 2005, **317**, 258–266.
36 C. Branca, S. Maccarrone, S. Magazu, G. Maisano, S. M. Bennington and J. Taylor, Tetrahedral Order in Homologous Disaccharide-Water Mixtures, *J. Chem. Phys.*, 2005, **122**, 174513.
37 S. Magazu, P. Migliardo, A. M. Musolino and M. T. Sciortino, α,α-Trehalose-Water Solutions. 1. Hydration Phenomena and Anomalies in the Acoustic Properties, *J. Phys. Chem. B*, 1997, **101**, 2348–2351.
38 C. Branca, S. Magazu, G. Maisano, F. Migliardo, P. Migliardo and G. Romeo, α,α-Trehalose/Water Solutions. 5. Hydration and Viscosity in Dilute and Semidilute Disaccharide Solutions, *J. Phys. Chem. B*, 2001, **105**, 10140–10145.
39 S. Magazu, V. Villari, P. Migliardo, G. Maisano and M. T. F. Telling, Diffusive Dynamics of Water in the Presence of Homologous Disaccharides: A Comparative Study by Quasi Elastic Neutron Scattering. IV, *J. Phys. Chem. B*, 2001, **105**, 1851–1855.
40 M. Paolantoni, L. Comez, M. E. Gallina, P. Sassi, F. Scarponi, D. Fioretto and A. Morresi, Light Scattering Spectra of Water in Trehalose Aqueous Solutions: Evidence for Two Different Solvent Relaxation Processes, *J. Phys. Chem. B*, 2009, **113**, 7874–7878.
41 U. Heugen, G. Schwaab, E. Bruendermann, M. Heyden, X. Yu, D. M. Leitner and M. Havenith, Solute-Induced Retardation of Water Dynamics Probed Directly by Terahertz Spectroscopy, *Proc. Natl. Acad. Sci. U. S. A.*, 2006, **103**, 12301–12306.
42 S. L. Lee, P. G. Debenedetti and J. R. Errington, A Computational Study of Hydration, Solution Structure, and Dynamics in Dilute Carbohydrate Solutions, *J. Chem. Phys.*, 2005, **122**, 204511.
43 C. J. Roberts and P. G. Debenedetti, Structure and Dynamics in Concentrated, Amorphous Carbohydrate-Water Systems by Molecular Dynamics Simulation, *J. Phys. Chem. B*, 1999, **103**, 7308–7318.
44 P. B. Conrad and J. J. de Pablo, Computer Simulation of the Cryoprotectant Disaccharide α,α-Trehalose in Aqueous Solution, *J. Phys. Chem. A*, 1999, **103**, 4049–4055.
45 N. C. Ekdawi-Sever, P. B. Conrad and J. J. de Pablo, Molecular Simulation of Sucrose Solutions near the Glass Transition Temperature, *J. Phys. Chem. A*, 2001, **105**, 734–742.
46 A. Lerbret, P. Bordat, F. Affouard, M. Descamps and F. Migliardo, How Homogeneous are the Trehalose, Maltose, and Sucrose Water Solutions? An Insight from Molecular Dynamics Simulations, *J. Phys. Chem. B*, 2005, **109**, 11046–11057.
47 F. Sussich, S. Bortoluzzi and A. Cesaro, Trehalose Dehydration under Confined Conditions, *Thermochim. Acta*, 2002, **391**, 137–150.
48 T. Furuki, A. Kishi and M. Sakurai, De- and Rehydration Behaviour of α,α-Trehalose Dihydrate under Humidity-Controlled Atmospheres, *Carbohydr. Res.*, 2005, **340**, 429–438.
49 K. Kawai, T. Hagiwara, R. Takai and T. Suzuki, Comparative Investigation by Two Analytical Approaches of Enthalpy Relaxation for Glassy Glucose, Sucrose, Maltose, and Trehalose, *Pharm. Res.*, 2005, **22**, 490–495.
50 R. Lefort, P. Bordat, A. Cesaro and M. Descamps, Exploring the Conformational Energy Landscape of Glassy Disaccharides by Cross Polarization Magic Angle Spinning C-13 Nuclear Magnetic Resonance and Numerical Simulations. II. Enhanced Molecular Flexibility in Amorphous Trehalose, *J. Chem. Phys.*, 2007, **126**, 014511.
51 G. I. Likhtenshtein, J. Yamauchi, S. Nakatsuji, A. I. Smirnov and R. Tamura, *Nitroxides: Applications in Chemistry, Biomedicine, and Materials Science*, Wiley-VCH, Weinheim, 2008.
52 H.-J. Steinhoff, A. Savitsky, C. Wegener, M. Pfeiffer, M. Plato and K. Möbius, High-field EPR Studies of the Structure and Conformational Changes of Site Directed Spin Labeled Bacteriorhodopsin, *Biochim. Biophys. Acta*, 2000, **1457**, 253–262.
53 M. Plato, H.-J. Steinhoff, C. Wegener, J. T. Törring, A. Savitsky and K. Möbius, Molecular Orbital Study of Polarity and Hydrogen Bonding Effects on the g and Hyperfine Tensors of Site Directed NO Spin Labeled Bacteriorhodopsin, *Mol. Phys.*, 2002, **100**, 3711.
54 E. Bordignon, H. Brutlach, L. Urban, K. Hideg, A. Savitsky, A. Schnegg, P. Gast, M. Engelhard, E. J. J. Groenen, K. Möbius and H. J. Steinhoff, Heterogeneity in the Nitroxide Micro-Environment: Polarity and Proticity Effects in Spin-Labeled Proteins Studied by Multi-Frequency EPR, *Appl. Magn. Reson.*, 2010, **37**, 391–403.
55 J. H. Freed, ESR and Molecular Dynamics, in *Biological Magnetic Resonance*, ed. S. R. Eaton, G. R. Eaton and L. J. Berliner, 2005, vol. 24, pp. 239–268.
56 S. K. Misra and J. H. Freed, Molecular Motions, *Multifrequency Electron Paramagnetic Resonance: Theory and Applications*, Wiley-VCH, Berlin, 2011, pp. 497–544.
57 K. Möbius and A. Savitsky, *High-Field EPR Spectroscopy on Proteins and their Model Systems: Characterization of Transient Paramagnetic States*, Royal Society of Chemistry, London, 2009.
58 Y. N. Molin, K. M. Salikhov and K. I. Zamaraev, *Spin Exchange. Principles and Applications in Chemistry and Biology*, Springer, Heidelberg, 1980.

59 A. Savitsky, A. A. Dubinskii, M. Plato, Y. A. Grishin, H. Zimmermann and K. Möbius, High-field EPR and ESEEM Investigation of the Nitrogen Quadrupole Interaction of Nitroxide Spin Labels in Disordered Solids: Towards Differentiation between Polarity and Proticity Matrix Effects on Protein Function, *J. Phys. Chem. B*, 2008, **112**, 9079–9090.

60 M. Malferrari, F. Francia and G. Venturoli, Coupling between Electron Transfer and Protein-Solvent Dynamics: FTIR and Laser-Flash Spectroscopy Studies in Photosynthetic Reaction Center Films at Different Hydration Levels, *J. Phys. Chem. B*, 2011, **115**, 14732–14750.

61 K. A. Gray, J. W. Farchaus, J. Wachtveitl, J. Breton and D. Oesterhelt, Initial Characterization of Site-Directed Mutants of Tyrosine M210 in the Reaction Center of *Rhodobacter-Sphaeroides*, *EMBO J.*, 1990, **9**, 2061–2070.

62 O. Burghaus, M. Rohrer, T. Götzinger, M. Plato and K. Möbius, A Novel High-Field High-Frequency EPR and ENDOR Spectrometer Operating at 3 Mm Wavelength, *Meas. Sci. Technol.*, 1992, **3**, 765–774.

63 T. F. Prisner, M. Rohrer and K. Möbius, Pulsed 95-GHz, High-Field EPR Heterodyne Spectrometer with High Spectral and Time Resolution, *Appl. Magn. Reson.*, 1994, **7**, 167–183.

64 K. Möbius, A. Savitsky, A. Schnegg, M. Plato and M. Fuchs, High-Field EPR Spectroscopy Applied to Biological Systems: Characterization of Molecular Switches for Electron and Ion Transfer, *Phys. Chem. Chem. Phys.*, 2005, **7**, 19–42.

65 P. R. Cullis, Electron-Paramagnetic Resonance in Inhomogeneously Broadened Systems – Spin Temperature Approach, *J. Magn. Reson.*, 1976, **21**, 397–418.

66 P. R. Cullis and J. R. Marko, Electron-Paramagnetic Resonance Properties of N-Type Silicon in Intermediate Impurity-Concentration Range, *Phys. Rev. B: Solid State*, 1975, **11**, 4184–4200.

67 Y. S. Lebedev, High-Frequency Continuous-Wave Electron Spin Resonance, in *Modern Pulsed and Continuous-Wave Electron Spin Resonance*, ed. L. Kevan and M. K. Bowman, John Wiley, New York, 1990, pp. 365–404.

68 S. Stoll and A. Schweiger, EasySpin, A Comprehensive Software Package for Spectral Simulation and Analysis in EPR, *J. Magn. Reson.*, 2006, **178**, 42–55.

69 S. Stoll and A. Schweiger, Easyspin: Simulating CW ESR spectra, in *ESR Spectroscopy in Membrane Biophysics*, ed. M. A. Hemminga and L. J. Berliner, Springer, New York, 2007, vol. 27, pp. 299–321.

70 P. R. Bevington, *Data Reduction and Error Analysis for the Physical Sciences*, McGraw-Hill, New York, 1969.

71 J. J. Max and C. Chapados, Isotope Effects in Liquid Water by Infrared Spectroscopy, *J. Phys. Chem.*, 2002, **116**, 4626–4642.

72 A. Nilsson, A. Holmgren and G. Lindblom, Fourier-Transform Infrared-Spectroscopy Study of Dioleoylphosphatidylcholine and Monooleoylglycerol in Lamellar and Cubic Liquid-Crystals, *Biochemistry*, 1991, **30**, 2126–2133.

73 S. Chiantia, L. I. Giannola and L. Cordone, Lipid Phase Transition in Saccharide-Coated Cholate-Containing Liposomes: Coupling to the Surrounding Matrix, *Langmuir*, 2005, **21**, 4108–4116.

74 Y. Marechal, The Molecular Structure of Liquid Water Delivered by Absorption Spectroscopy in the whole IR Region Completed with Thermodynamics Data, *J. Mol. Struct.*, 2011, **1004**, 146–155.

75 S. A. Dzuba, E. S. Salnikov and L. V. Kulik, CW EPR, Echo-Detected EPR, and Field-Step ELDOR Study of Molecular Motions of Nitroxides in o-Terphenyl Glass: Dynamical Transition, Dynamical Heterogeneity and Beta-Relaxation, *Appl. Magn. Reson.*, 2006, **30**, 637–650.

76 A. Savitsky, M. Plato and K. Möbius, The Temperature Dependence of Nitroxide Spin-Label Interaction Parameters: a High-Field EPR Study of Intramolecular Motional Contributions, *Appl. Magn. Reson.*, 2010, **37**, 415–434.

77 I. Peric, D. Merunka, B. L. Bales and M. Peric, Rotation of Four Small Nitroxide Probes in Supercooled Bulk Water, *J. Phys. Chem. Lett.*, 2013, **4**, 508–513.

78 M. V. Galmarini, R. Baeza, V. Sanchez, M. C. Zamora and J. Chirife, Comparison of the Viscosity of Trehalose and Sucrose Solutions at Various Temperatures: Effect of Guar Gum Addition, *Food Sci. Technol.*, 2011, **44**, 186–190.

79 N. Ekdawi-Sever, J. J. de Pablo, E. Feick and E. von Meerwall, Diffusion of Sucrose and α,α-Trehalose in Aqueous Solutions, *J. Phys. Chem. A*, 2003, **107**, 936–943.

80 T. Uchida, M. Nagayama and K. Gohara, Trehalose Solution Viscosity at Low Temperatures Measured by Dynamic Light Scattering Method: Trehalose Depresses Molecular Transportation for Ice Crystal Growth, *J. Cryst. Growth*, 2009, **311**, 4747–4752.

81 M. Rampp, C. Buttersack and H. D. Ludemann, c,T-Dependence of the Viscosity and the Self-Diffusion Coefficients in Some Aqueous Carbohydrate Solutions, *Carbohydr. Res.*, 2000, **328**, 561–572.

82 A. Longo, S. Giuffrida, G. Cottone and L. Cordone, Myoglobin Embedded in Saccharide Amorphous Matrices: Water-Dependent Domains Evidenced by Small Angle X-Ray Scattering, *Phys. Chem. Chem. Phys.*, 2010, **12**, 6852–6858.

83 B. Roser, Trehalose Drying – A Novel Replacement for Freeze-Drying, *Biopharm*, 1991, **4**, 47–52.

84 C. Colaco, S. Sen, M. Thangavelu, S. Pinder and B. Roser, Extraordinary Stability of Enzymes Dried in Trehalose – Simplified Molecular-Biology, *Biotechnology*, 1992, **10**, 1007–1011.

85 M. Uritani, M. Takai and K. Yoshinaga, Protective Effect of Disaccharides on Restriction Endonucleases During Drying Under Vacuum, *J. Biochem.*, 1995, **117**, 774–779.

86 G. Feher, J. P. Allen, M. Y. Okamura and D. C. Rees, Structure and Function of Bacterial Photosynthetic Reaction Centers, *Nature*, 1989, **339**, 111–116.

87 A. J. Hoff and J. Deisenhofer, Photophysics of Photosynthesis. Structure and Spectroscopy of Reaction Centers of Purple Bacteria, *Phys. Rep.*, 1997, **287**, 1–247.

88 D. Kleinfeld, M. Y. Okamura and G. Feher, Electron-Transfer Kinetics in Photosynthetic Reaction Centers

Cooled to Cryogenic Temperatures in the Charge-Separated State: Evidence for Light-Induced Structural Changes, *Biochemistry*, 1984, **23**, 5780–5786.

89 B. H. McMahon, J. D. Muller, C. A. Wraight and G. U. Nienhaus, Electron Transfer and Protein Dynamics in The Photosynthetic Reaction Center, *Biophys. J.*, 1998, **74**, 2567–2587.

90 G. Palazzo, A. Mallardi, A. Hochkoeppler, L. Cordone and G. Venturoli, Electron Transfer Kinetics in Photosynthetic Reaction Centers Embedded in Trehalose Glasses: Trapping of Conformational Substates at Room Temperature, *Biophys. J.*, 2002, **82**, 558–568.

91 F. Francia, G. Palazzo, A. Mallardi, L. Cordone and G. Venturoli, Probing Light-Induced Conformational Transitions in Bacterial Photosynthetic Reaction Centers Embedded in Trehalose-Water Amorphous Matrices, *Biochim. Biophys. Acta*, 2004, **1658**, 50–57.

92 H. Frauenfelder, G. Chen, J. Berendzen, P. W. Fenimore, H. Jansson, B. H. McMahon, I. R. Stroe, J. Swenson and R. D. Young, A Unified Model of Protein Dynamics, *Proc. Natl. Acad. Sci. U. S. A.*, 2009, **106**, 5129–5134.

